

## **Anonymous Referee #1**

Received and published: 20 April 2017

This manuscript describes a detailed sensitivity simulation of CH<sub>4</sub>/CO<sub>2</sub> in Asia with respect to horizontal resolution employing two different versions of the LMDzINCA model. This kind of study can be expected to contribute significantly to improving performance of data assimilation and accuracy of inverse modeling as the authors emphasize. The overall text is well written, and the authors very carefully discuss the results. However, most of the descriptions in this paper appear to be too detailed and sometime tedious although they may be needed to convey useful information to the data assimilation procedure. The subject of this paper seems to be appropriate to the ACP. However, I would like the authors to consider my questions and revise the manuscript before I recommend the publication of this paper. Details of my comments will be found in the following.

**[Response]** Thank you very much for your careful review and comments. Following the reviewers' suggestions, we launched new simulations with 39 vertical layers (L39) for both standard and zoom models, as compared to the previous simulations with only 19 vertical layers (L19). We updated the biomass burning emissions to the latest GFEDv4.1 for both CH<sub>4</sub> and CO<sub>2</sub> simulations. For CH<sub>4</sub>, we also ran sensitivity test simulations, in which anthropogenic and wetland emissions are prescribed with the latest EDGARv4.3.2 and model outputs from ORCHIDEE. For CO<sub>2</sub>, sensitivity test simulations are also performed with daily and 3-hourly biomass burning emissions from GFEDv4.1 (Table R1). We have rewritten most part of the results, discussions and conclusions accordingly. We also replied to your major and minor comments in the following, and hopefully our responses and revision adequately address all your comments and questions.

### **Major Comments:**

M1: For “abstract” and “conclusions” section, I’m not convinced about conclusions of this manuscript. The authors state that the finer horizontal resolution version improves Asian CH<sub>4</sub>/CO<sub>2</sub> simulation only moderately. Are you saying that enhancing horizontal resolution is not that useful (not beneficial)? I think you could more clearly express the message/implication of this study at least in abstract and conclusions parts.

**[Response]** Not really. The model's capability to represent the CH<sub>4</sub> or CO<sub>2</sub> variability at stations does not only depend on model resolution. In this paper we would like to more emphasize that, with finer model resolution, the model performance is more sensitive to accuracy of the prescribed surface fluxes, particularly distribution of sources/sinks at fine scales and their short-term variabilities. The sensitivity test simulations we launched for the revised paper also show importance of the flux data quality in model performance and thus benefits of improved model resolution. Following your suggestion, we revised the manuscript and clarify it in Abstract and Conclusion.

M2: This study just showed that a finer horizontal resolution more or less contributes to improvement of CH<sub>4</sub>/CO<sub>2</sub> simulation for Asia. But it is very unclear whether this improvement is really significant or meaningful in terms of regional budget and flux estimate. I think the authors should check the impacts of other factors (at least vertical resolution or NEE) on the simulation as well as horizontal resolution for more clearly appealing the advantages of your zoomed method in the LMDzINCA modeling framework.

**[Response]** As we stated in Introduction, the number of regional ground stations in South and East Asia has increased during the recent decades. Observations from these stations will provide useful constraints on regional flux estimates, if gradients between stations and their variabilities can be well represented in transport models. Compared to the global transport model with rather coarse model resolution, the zoomed transport model used in our study has the potential to better capture the observed spatial and temporal variations at regional stations due to the reduced representation errors. The impact of model resolution on regional budget and flux estimate should be addressed by inverse modeling, which is beyond the scope of this study. Following your suggestion, we launched new simulations with 39 vertical layers (L39) for both standard and zoom models, as compared to the previous simulations with only 19 vertical layers (L19). For CH<sub>4</sub>, we also ran sensitivity test simulations, in which anthropogenic and wetland emissions are prescribed with the latest EDGARv4.3.2 and model outputs from ORCHIDEE (Table R1). Detailed results and discussions are presented in Section 3 in the revised manuscript.

M3: For the moderate improvement with ZASIA, I do not yet understand the reason for it. The authors give several potential candidates like matching between the model's grid and observation site, different transport, etc. But how much do they contribute? Or what is the most possible reason for the improvement?

**[Response]** With the zoomed model, the explanation for the improved model performance on CH<sub>4</sub> mean annual gradients really depends on different stations. As mentioned in Section 3.1.1, the better performance at SDZ (117.12°E, 40.65°N, 293m a.s.l.) is more related to the detailed description of source distribution around the station; for the two coastal stations PON (79.86°E, 12.01°N, 30m a.s.l.) and CRI (73.83°E, 15.08°N, 66m a.s.l.), the improved model performance is related to the better characterization of the complex terrain (coastal topography) as well as the fluxes.

M4: The authors stated that the ZASIA version does not deteriorate the performance of CH<sub>4</sub>/CO<sub>2</sub> outside the zoomed area (L383). But they seem to be looking only at the sites displayed in Figure 1 (mostly in Japan). How about the impacts on performance for other sites like in EU, US, Africa, and the southern hemisphere? This point should be clarified in the main text with an additional figure as supplementary material.

**[Response]** Following your suggestions, we further included several global/regional stations in Europe (the stations JFJ and MHD), North America (the stations ALT, BRW, NWR and

MLO), and the southern hemisphere (the stations AMS, CGO, and SPO) in this study (Table 2). Analyses show that the zoom versions do not deteriorate model performance outside the zoomed region compared to the standard versions. For example, the CH<sub>4</sub> and CO<sub>2</sub> annual gradients between HLE and these added stations can be well captured by both standard and zoom model versions (see open circles in Figure 2). Detailed results and discussions are presented in Section 3 and the supplementary material.

### **Minor Comments:**

L158 to L173: How do you represent diurnal variation in OH?

**[Response]** As described in Section 2.1.1, we used climatological monthly OH concentration fields in this study and didn't consider the diurnal variation in OH fields. According to Patra et al. (2009), the CH<sub>4</sub> chemical lifetime in the troposphere is much longer than the dynamical residence time due to atmospheric transport, and accounting for OH diurnal cycle is not crucial for simulating seasonal, synoptic, and diurnal variations in CH<sub>4</sub> concentration fields.

L177 "The spin-up time of 6 years": Don't you have any trend or drift of global mean CH<sub>4</sub> concentration during these 6 years?

**[Response]** Take the global background station Mauna Loa as an example, Figure R1 presents time series of the simulated and observed CH<sub>4</sub> concentrations over the period 2000–2013, as well as the corresponding long term trends extracted from the data using the CCGVU curve fitting routine (Thoning et al., 1989). During the 6-year spin-up period (2000–2005), the simulated CH<sub>4</sub> concentrations decreased for the first three years and then levelled off. Drift of the global mean is found for both standard and zoom models, equivalent to around -12 ppb over this period. The model-observation disagreement in trend and global mean CH<sub>4</sub> concentrations results from the imperfect surface emissions and OH fields prescribed in the simulations. As we reply to the Reviewer #2 (Specific comments, Line 163), in this paper we are more focusing on the improvement gained from refinement of model grids rather than accurately reproducing the observed CH<sub>4</sub> concentrations and their interannual variations. Furthermore, all the traits and metrics we have considered to evaluate the model performance (i.e., annual mean gradient, seasonal cycle, synoptic variability, diurnal cycle and vertical gradient) give "relative" values that are not affected by the absolute CH<sub>4</sub> concentrations. Therefore the trend and drift of global mean CH<sub>4</sub> during the spin-up period will not have significant impact on comparison of performance between the standard and zoom models.

L179 "already realistic": What do you mean by "realistic"? You should explain more about the initial conditions for CH<sub>4</sub>.

**[Response]** In the revised paper, the initial CH<sub>4</sub> concentration field we used for the updated simulations is defined based on the optimized initial state from a CH<sub>4</sub> inversion that assimilates observations from 50+ global background stations over the period 2006–2012

(Locatelli, 2014; Locatelli et al., 2015). The optimized initial CH<sub>4</sub> concentration field for the year 2006 was rescaled to the levels of the year 2000 and used as the initial state in our simulations. As the initial condition for CH<sub>4</sub> is optimized with observations, we assume it to be “realistic”. Following your suggestion, we revised Section 2.1.1 accordingly to clarify the setup of initial condition for CH<sub>4</sub>.

L395 “better description of the surface fluxes and/or transport”: Given the fact that CO<sub>2</sub> simulation is not improved by ZASIA, the improvement seen in CH<sub>4</sub> seems to be resulting from non-transport process (surface fluxes?).

**[Response]** Here we mean that, with ZASIA, the model improvement on the CH<sub>4</sub> annual gradient at the stations SDZ, PON and CRI may “result from a reduction in representation error with a higher model horizontal resolution in the zoomed region, through a better description of the surface fluxes and/or transport around these stations”. In fact, we also found improved model performance on the CO<sub>2</sub> annual gradients at the three stations, although not as significant as it is for CH<sub>4</sub> (Table R2). Therefore the model improvement may result from better characterization of either surface fluxes or transport processes or both.

L435: There appears no explanation for the abbreviation of “NEE”.

**[Response]** Following your suggestions, we provide the full name (net ecosystem exchange) when the abbreviation is used for the first time.

L500 “rather coarse (19 layers)”: How do you get the model concentrations at the elevation of the observational site? The model layers are linearly interpolated?

**[Response]** As described in Section 2.3, the modelled concentrations are sampled at the nearest gridpoint and vertical level to each station.

## Tables

**Table R1** Model setups for different simulations.

Simulation Code	Version	Anthrop. Emis.	Wetland Emis.
ST19_ED42	144×142 Standard, 19 layers	EDGAR4.2FT2010	KAPLAN climatology
ZA19_ED42	144×142 Asian Zoom, 19 layers		
ST39_ED42	144×142 Standard, 39 layers		
ZA39_ED42	144×142 Asian Zoom, 39 layers		
ST39_ED432	144×142 Standard, 19 layers	EDGAR4.3.2	ORCHIDEE climatology
ZA39_ED432	144×142 Asian Zoom, 19 layers		
ST39_ED432ORC	144×142 Standard, 39 layers		
ZA39_ED432ORC	144×142 Asian Zoom, 39 layers		

**Table R2** The observed and simulated mean annual gradient of CH<sub>4</sub> (a) and CO<sub>2</sub> (b) between HLE and two stations (CRI, PON and SDZ) within the zoomed region. The bias reduction rates (in percentage) by using ZA compared to ST are also given for both 19- and 39-layer simulations.

a)

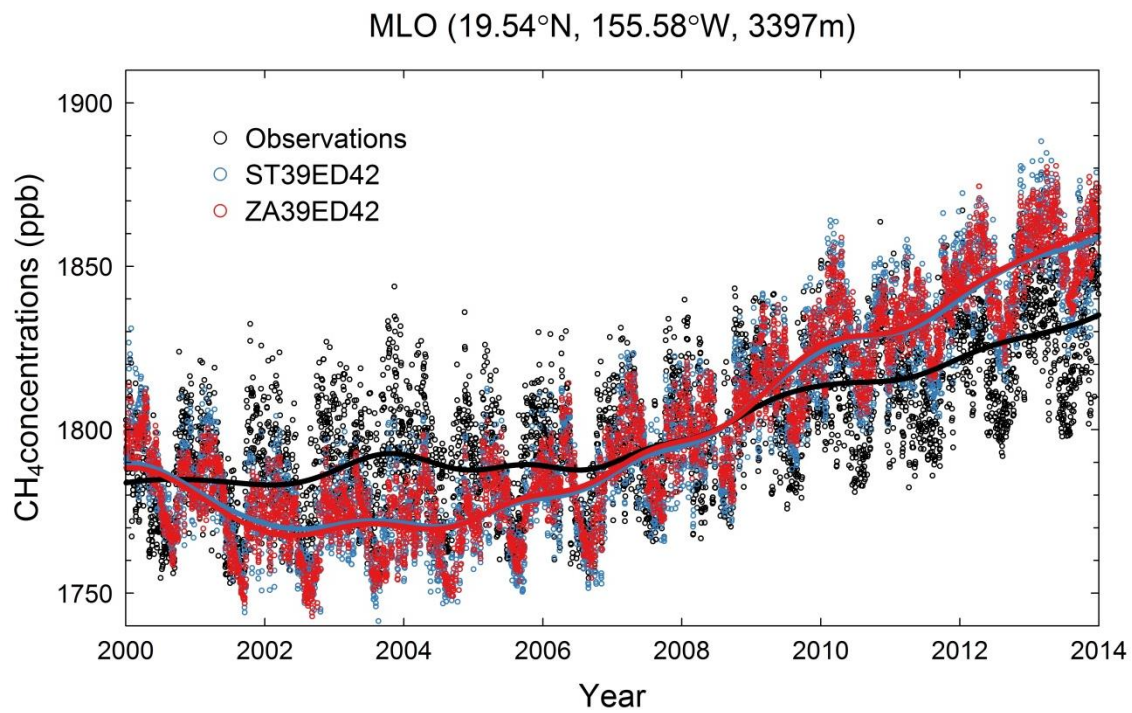
CH <sub>4</sub>	OBS (ppb)	ST19 (ppb)	ZA19 (ppb)	Bias reduction	ST39 (ppb)	ZA39 (ppb)	Bias reduction
CRI	17.5±12.7	9.3±4.1	20.2±7.1	66.6%	8.6±3.0	23.0±6.7	38.8%
PON	32.4±12.4	2.5±11.6	31.1±7.7	95.6%	0.4±11.9	34.1±7.8	94.7%
SDZ	90.0±15.4	125.1±18.8	86.8±16.0	91.0%	128.5±19.3	100.4±22.4	73.0%

b)

CO <sub>2</sub>	OBS (ppm)	ST19 (ppm)	ZA19 (ppm)	Bias reduction	ST39 (ppm)	ZA39 (ppm)	Bias reduction
CRI	4.6±0.9	1.2±0.1	2.0±0.3	25.5%	1.4±0.1	2.2±0.2	25.2%
PON	2.7±1.6	1.3±0.3	1.8±0.5	35.2%	1.5±0.3	1.9±0.5	37.0%
SDZ	6.8±0.5	8.8±1.3	7.7±1.9	57.9%	9.3±1.5	8.1±2.3	48.1%

## Figures

**Figure R1** Time series of observed and simulated CH<sub>4</sub> concentrations at Mauna Loa (MLO, 19.54°N, 155.58°W, 3397) during the period 2000–2013. The simulated CH<sub>4</sub> concentrations are based on outputs from both standard (ST39ED42, blue circles) and zoom models (ZA39ED42, red circles). The solid lines indicate the corresponding long-term trends extracted from the data using the CCGVU curve-fitting routine (Thoning et al., 1989).



## References

Locatelli, R.: Estimation des sources et puits de méthane: bilan planétaire et impacts de la modélisation du transport atmosphérique, Versailles-St Quentin en Yvelines, France. [online] Available from: <http://www.theses.fr/2014VERS0035>, 2014.

Locatelli, R., Bousquet, P., Saunois, M., Chevallier, F. and Cressot, C.: Sensitivity of the recent methane budget to LMDz sub-grid-scale physical parameterizations, *Atmos. Chem. Phys.*, 15, 9765–9780, doi:10.5194/acp-15-9765-2015, 2015.

Patra, P., Takigawa, M., Ishijima, K., Choi, B.-C., Cunnold, D., J. Dlugokencky, E., Fraser, P., J. Gomez-Pelaez, A., Goo, T.-Y., Kim, J.-S., Krummel, P., Langenfelds, R., Meinhardt, F., Mukai, H., O'Doherty, S., G. Prinn, R., Simmonds, P., Steele, P., Tohjima, Y., Tsuboi, K., Uhse, K., Weiss, R., Worthy, D. and Nakazawa, T.: Growth rate, seasonal, synoptic, diurnal variations and budget of methane in the lower atmosphere, *J. Meteorol. Soc. Japan*, 87(4), 635–663, doi:10.2151/jmsj.87.635, 2009.

Thoning, K. W., Tans, P. P. and Komhyr, W. D.: Atmospheric carbon dioxide at Mauna Loa Observatory: 2. Analysis of the NOAA GMCC data, 1974–1985, *J. Geophys. Res. Atmos.*, 94(D6), 8549–8565, doi:10.1029/JD094iD06p08549, 1989.

Anonymous Referee #2

Received and published: 28 April 2017

This study presents a detailed comparison between CO<sub>2</sub> and CH<sub>4</sub> simulations from the LMDzINCA model and the available measurements over South East Asia. It is meant as a first step in preparation for flux inversions, to identify observed signals pointing to shortcomings in the a priori fluxes or transport model uncertainty, in support of the inversion set-up. To this end a comparison is made between different model versions, and the added value of increased model resolution is assessed. The manuscript is well written, and the difference between model and measurements is carefully assessed. However, there should be a more efficient way to arrive at the main conclusions, e.g. by summarizing the performance in only a few key figures. This would also help to make the final conclusions more quantitative. In its current form, the scientific message is not so clear. In my opinion, publication in ACP would require more than just model performance documentation. Therefore, additional effort is needed to strengthen the scientific significance of this work.

**[Response]** Thank you very much for your careful review and comments. Following the reviewers' suggestions, we launched new simulations with 39 vertical layers (L39) for both STs and ZAs, as compared to the previous simulations with only 19 vertical layers (L19). We updated the biomass burning emissions to the latest GFEDv4.1 for both CH<sub>4</sub> and CO<sub>2</sub> simulations. For CH<sub>4</sub>, we also ran sensitivity test simulations, in which anthropogenic and wetland emissions are prescribed with the latest EDGARv4.3.2 and model outputs from ORCHIDEE. For CO<sub>2</sub>, sensitivity test simulations are also performed with daily and 3-hourly biomass burning emissions from GFEDv4.1 (Table R1). Following your suggestions, we have rewritten most part of results, discussions and conclusions in the manuscript accordingly. We also replied to your major and minor comments in the following, and hopefully our responses and revision adequately address all your comments and questions.

#### GENERAL COMMENTS

The conclusions describe the performance of the two model versions in qualitative, and sometimes rather vague, terms such as 'generally capable', 'moderately improves', 'fairly well', etc. Some key numbers are needed quantifying the performance, and the significance of performance differences. For example, one would expect improved resolution to pay out more on performance metrics addressing short-term variability, or at sites that are more influenced by small scale variability in the sources and sinks. Different temporal scales are addressed separately, but, to improve the scientific significance, the relation between them could be addressed in further detail.

**[Response]** Following your suggestion, we have rewritten the conclusions and implications. Key numbers are given with respect to the model improvement with finer horizontal resolution. We also claim that the performance of high resolution transport model is more



sensitive to errors in meteorological forcings and surface fluxes, especially when short-term variabilities or stations close to source regions are examined. This emphasizes importance of accurate a priori CH<sub>4</sub> surface fluxes in high resolution transport modelling and inverse studies, particularly regarding locations and magnitudes of emission hotspots. Please refer to Section 4 for more details.

The idea to compare CO<sub>2</sub> and CH<sub>4</sub> is interesting, however, it is difficult to compare the model performance between the two. It is like comparing apples and oranges, since the spatio-temporal scales that are influenced by the emissions of these tracers in relation to variations due to transport are so different. It is suggested that the emission uncertainty is more important for CO<sub>2</sub> than for CH<sub>4</sub>, but because of the correlation between flux and transport uncertainties (e.g. the rectifier in case of CO<sub>2</sub>) it is not possible to really separate these influences. If without this problem, the question remains what it means for the potential of the inversion to contribute to our understanding of the fluxes. The results suggest that this potential is better for CO<sub>2</sub>, whereas I don't think this can really be objectively quantified just from forward simulations.

**[Response]** We agree with Reviewer #2 that it's difficult to compare the model performance between CO<sub>2</sub> and CH<sub>4</sub>, and that the correlation between flux and transport uncertainty is not possible to be really separated. In the revised paper we no longer suggest the emission uncertainty is more important for CO<sub>2</sub> than for CH<sub>4</sub>. In fact, the emission uncertainty is important for both gases, yet in different ways. For CH<sub>4</sub>, we highlight importance of uncertainty regarding the magnitudes and distribution of emission hotspots; while with respect to CO<sub>2</sub>, we more focus on uncertainties related to the spatio-temporally varying NEE fluxes. We rephrased the conclusions and implications in Section 4 and removed statements about the potential of inversions to contribute to our understanding of CO<sub>2</sub> or CH<sub>4</sub> fluxes. However, in a few places we kept comparisons between CO<sub>2</sub> and CH<sub>4</sub> at specific stations. For example, in Section 3.2, the strong contrast in model performance between CO<sub>2</sub> and CH<sub>4</sub> seasonal cycles at BKT does suggest inaccurate seasonal variations in the prescribed CO<sub>2</sub> surface fluxes such as NEE.

I see the value of assessing the benefits of improving model resolution. The trouble here, however, is the limiting vertical resolution. The conclusion that this resolution needs to be improved seems quite obvious to me, to the extent that I even wonder why this was not done from the start. It seems a necessary prerequisite for assessing the benefits of improved model resolution.

**[Response]** Following your suggestion, we launched new simulations with 39 vertical layers (L39) for both STs and ZAs, as compared to the previous simulations with only 19 vertical layers (L19). The detailed model setups for control simulations and sensitivity tests prescribed with different surface fluxes are shown in Table R1. In brief, increasing model vertical resolution does not have as much impact on model performance as increasing the horizontal resolution at any temporal scale, although in several cases the combination of finer

horizontal and vertical resolution tends to further increase the simulated amplitudes of variations (not necessarily improve the model performance). More detailed results and discussions are presented in Section 3.

Why has the vertical profile comparison to CONTRAIL been limited to CO<sub>2</sub>? It is true that CH<sub>4</sub> was measured only on a small subset of samples, but to include this could nevertheless be important to separate the influence of diurnal variations in emissions and PBL mixing. To me it seems that there is also some unexplored potential comparing diurnal cycle mismatches between CH<sub>4</sub> (PBL mixing controlled) and CO<sub>2</sub> (PBL mixing and flux variation controlled).

**[Response]** We agree that the model-data comparison of vertical profiles for both CO<sub>2</sub> and CH<sub>4</sub> would be important to separate the influence of diurnal variations in surface fluxes and PBL mixing. The question here is that the vertical profiles from the CONTRAIL project are only limited to CO<sub>2</sub> measurements that are made by on-board continuous measurement equipment (CME). Measurements for CH<sub>4</sub> are also available, but they are only flask samples in the high troposphere and stratosphere. Please refer to Machida et al. (2008) for further information about the project and the dataset.

Since the aim was to prepare for inversions, what are the implications of this study for the inversion setup? I mean, the implications that are mentioned don't seem to have any practical consequences (except for the need for improved vertical resolution).

**[Response]** There are three implications for inversion setup, which we have elaborated in Section 4. First, the performance of high resolution transport model is more sensitive to accuracy of the prescribed surface fluxes, especially regarding locations and magnitudes of emission hotspots for CH<sub>4</sub>. Therefore, one should be cautious when choosing an emission map as a priori for inversions. In particular, the unrealistic emission hotspots close to a station (as shown for UUM in Section 3.3.1) should be corrected, otherwise the inverted surface fluxes are likely to be strongly biased.

Second, as current bottom-up estimates of CH<sub>4</sub> sources and sinks still suffer from large uncertainties at fine scales, caution should be taken when one attempts to assimilate observations not realistically simulated by the high resolution transport model. These observations should be either removed from inversions or allocated with large uncertainties.

Third, representation of short-term variabilities is limited by model's ability to simulate boundary layer mixing and mesoscale transport in complex terrains. The recent implementation of new sub-grid physical parameterizations in LMDz is able to significantly improve simulation of the daily maximum during nighttime and thus diurnal cycles of tracer concentrations (Locatelli et al., 2015). To fully take advantage of high-frequency CH<sub>4</sub> or CO<sub>2</sub> observations at stations close to source regions, it is highly recommended to implement the new boundary layer physics in the current transport model, in addition to refinement of model horizontal and vertical resolutions. The current transport model with old planetary boundary

physics is not capable to capture diurnal variations at continental or mountain stations, therefore only observations that are well represented should be selected and kept for inversions (e.g. afternoon measurements for continental stations and nighttime measurements for mountain stations).

#### SPECIFIC COMMENTS

Line 163: How is the OH scaling done? A single scaling factor?

**[Response]** In the revised paper, we relaunch CH<sub>4</sub> simulations with different model versions, using OH fields regridded from outputs of a full chemistry INCA with model grids of 96×95×39. We don't scale the OH fields as did before to match the simulated global CH<sub>4</sub> growth rate with the observed one, as we are more focusing on the improvement gained from finer model resolutions rather than accurately reproducing the observed CH<sub>4</sub> concentrations and their interannual variations. Furthermore, all the traits and metrics we have considered to evaluate the model performance (i.e., annual mean gradient, seasonal cycle, synoptic variability, diurnal cycle and vertical gradient) give “relative” values that are not affected by the absolute CH<sub>4</sub> concentrations. Therefore the influences of the OH fields on the model improvement are assumed to be very small, and we don't scale them in the current CH<sub>4</sub> simulations. We revised the description of the OH fields accordingly in Section 2.1.1.

Line 194: Given the inter-annual variability of biomass burning, wouldn't it be better to use a climatological mean emission distribution for the extrapolated years?

**[Response]** In the updated simulations, we used GFEDv4.1 for emissions from biomass burning that are available over the whole running period (2000–2013). We revised the description of the prescribed surface fluxes accordingly in Section 2.1.2.

Section 2.2: Differences between calibration scales are mentioned but except for AMY CH<sub>4</sub> it is not clear how these differences have been accounted for.

**[Response]** As we described in Section 2.2, the CH<sub>4</sub> measurements at AMY are reported on the KRISS scale and they are not traceable to the WMO scale. For analyses of the CH<sub>4</sub> annual gradients between stations, we discard AMY because calibrations scales for different stations (i.e. AMY and HLE in this case) should be consistent for the calculation of gradients between them. For the analyses of seasonal cycle, synoptic variability and diurnal cycle, since the calibration scale doesn't significantly impact the results, we keep this station in these analyses.

Line 364: Is this after subtracting longer term components?

**[Response]** Yes. When we evaluated the model performance on CH<sub>4</sub> and CO<sub>2</sub> diurnal cycle, for each station daily means are subtracted from the raw data to remove any influence of

interannual, seasonal or even synoptic variations. We revised Section 2.4.4 in the manuscript to clarify it.

Line 408: Given the short regional transport times it is unclear how errors in OH could play a role.

**[Response]** The main sink of CH<sub>4</sub> is oxidation by OH in the troposphere. Although we agree that the regional transport time is much shorter compared to the CH<sub>4</sub> lifetime, the spatial (both horizontally and vertically) and seasonal distribution of OH can influence the model performance on CH<sub>4</sub> annual gradients between stations and seasonal cycles. Here in the paper, the CH<sub>4</sub> annual gradient between TAP and HLE is significantly overestimated by both STs and ZAs. The overall poor performance at this station suggests the prescribed surface emissions are probably overestimated over the station's footprint area (also shown by overestimation of seasonal amplitude at TAP), yet errors in OH distribution may also play a role – although we are not clear about the magnitude. To address the question we need an inverse system that can optimized the OH fields by assimilating observations of a tracer with well-known fluxes (e.g., methylchloroform), which is beyond the scope of this study.

Line 627: Would the improvements in PBL dynamics that are mentioned work in the right direction?

**[Response]** Yes. In Locatelli et al. (2015) the authors evaluated the impact of new physical parameterizations recently implemented in LMDz on representation of trace gas transport and chemistry. These development and modification on physical parameterization are to improve simulation of vertical diffusion, mesoscale mixing by thermal plumes in the planetary boundary layer (PBL), and deep convection in the troposphere. Regarding the PBL dynamics, the thermal plume model is developed and combined with Yamada (1983) diffusion scheme to improve representation of the diurnal cycles of thermodynamical and dynamical variables of the boundary layer and of shallow cumulus clouds (Hourdin et al., 2002; Rio et al., 2008). Locatelli et al. (2015) showed that implementing this new PBL physics in LMDz significantly improves representation of the daily peak values of <sup>222</sup>Rn concentrations at continental stations compared to the old model version (see Figure 3 in their paper), and the simulated diurnal cycles can agree very well with the observed one at a few tested stations (e.g. Heidelberg, as shown in Figure 4 in their paper). So far we haven't implemented the new PBL physics in our current model simulations, we will explore its potential in representation diurnal cycle of CO<sub>2</sub> and CH<sub>4</sub> in future studies.

Table 1: How about the seasonal variation in anthropogenic CH<sub>4</sub> emissions? (why are they taken into account for CO<sub>2</sub> but not for CH<sub>4</sub>?). How about the temporal variability of biomass burning? It seems relevant to make use of available information regarding its sub-monthly variability, in particular when assessing the impact of improved resolution is an important goal.

**[Response]** For the first question, we have considered the seasonal variation in anthropogenic CH<sub>4</sub> emissions from rice cultivation based on Matthews et al. (1991), as described in Section 2.1.2 and Table 1. The seasonal variations for other emission sectors are much smaller compared to those from rice paddies, and monthly sector-specific dataset is currently not available for the whole study period. Therefore we didn't considered seasonal variations in CH<sub>4</sub> emissions from those sectors. We revised Section 2.1.2 to further clarify it.

For the second question, in this study we used monthly biomass burning dataset from the GFEDv4.1 product. We agree that including its sub-monthly variability would be relevant when assessing the impact of increased resolution on model performance, especially for those stations that are potentially influenced by episodic large biomass burning events. Following your suggestion, we launched sensitivity test simulations for CO<sub>2</sub> using daily and 3-hourly biomass burning emissions for the year 2013, and evaluate the model performance on synoptic variation and diurnal cycle at a tropical station located in western Indonesia BKT (100.32°E, 0.20°S, 869m a.s.l.). Results show that simulations prescribed with daily or 3-hourly variability of biomass burning do not always improve representation of CO<sub>2</sub> diurnal cycle at BKT – sometimes could be worse, which again emphasizes uncertainties in prescribed surface fluxes (including uncertainties in temporal variability) as one of major factors that influence the model performance.

#### TECHNICAL CORRECTIONS

Line 132: 'representthe'

**[Response]** We corrected it.

Line 612: 'Here', where?

**[Response]** We rewrote the whole section. Please refer to Section 3.4.1.

S4: Why does the legend show blue colors? It would be better to leave this part out given that positive hotspots are in blue also.

**[Response]** Following your suggestion, we corrected the legend in Figure S4.

## References

- Hourdin, F., Couvreux, F., Menut, L., Hourdin, F., Couvreux, F. and Menut, L.: Parameterization of the Dry Convective Boundary Layer Based on a Mass Flux Representation of Thermals, *J. Atmos. Sci.*, 59(6), 1105–1123, doi:10.1175/1520-0469(2002)059<1105:POTDCB>2.0.CO;2, 2002.
- Locatelli, R., Bousquet, P., Hourdin, F., Saunois, M., Cozic, A., Couvreux, F., Grandpeix, J.-Y., Lefebvre, M.-P., Rio, C., Bergamaschi, P., Chambers, S. D., Karstens, U., Kazan, V., Van Der Laan, S., Meijer, H. A. J., Moncrieff, J., Ramonet, M., Scheeren, H. A., Schlosser, C., Schmidt, M., Vermeulen, A. and Williams, A. G.: Atmospheric transport and chemistry of trace gases in LMDz5B: evaluation and implications for inverse modelling, *Geosci. Model Dev*, 8, 129–150, doi:10.5194/gmd-8-129-2015, 2015.
- Machida, T., Matsueda, H., Sawa, Y., Nakagawa, Y., Hirokuni, K., Kondo, N., Goto, K., Nakazawa, T., Ishikawa, K. and Ogawa, T.: Worldwide measurements of atmospheric CO<sub>2</sub> and other trace gas species using commercial airlines, *J. Atmos. Ocean. Technol.*, 25(10), 1744–1754, doi:10.1175/2008JTECHA1082.1, 2008.
- Matthews, E., Fung, I. and Lerner, J.: Methane emission from rice cultivation: Geographic and seasonal distribution of cultivated areas and emissions, *Global Biogeochem. Cycles*, 5(1), 3–24, doi:10.1029/90GB02311, 1991.
- Rio, C., Hourdin, F., Rio, C. and Hourdin, F.: A Thermal Plume Model for the Convective Boundary Layer: Representation of Cumulus Clouds, *J. Atmos. Sci.*, 65(2), 407–425, doi:10.1175/2007JAS2256.1, 2008.
- Yamada, T.: Simulations of Nocturnal Drainage Flows by a  $q^2$  Turbulence Closure Model, *J. Atmos. Sci.*, 40(1), 91–106, doi:10.1175/1520-0469(1983)040<0091:SONDFB>2.0.CO;2, 1983.

## Tables

**Table R1** Model setups for different simulations.

Simulation Code	Version	Anthrop. Emis.	Wetland Emis.
ST19_ED42	144×142 Standard, 19 layers	EDGAR4.2FT2010	KAPLAN climatology
ZA19_ED42	144×142 Asian Zoom, 19 layers		
ST39_ED42	144×142 Standard, 39 layers		
ZA39_ED42	144×142 Asian Zoom, 39 layers		
ST39_ED432	144×142 Standard, 19 layers	EDGAR4.3.2	ORCHIDEE climatology
ZA39_ED432	144×142 Asian Zoom, 19 layers		
ST39_ED432ORC	144×142 Standard, 39 layers		
ZA39_ED432ORC	144×142 Asian Zoom, 39 layers		

1 **Simulating CH<sub>4</sub> and CO<sub>2</sub> over South and East Asia using the zoomed**  
2 **chemistry transport model LMDzINCA**

3 Xin Lin<sup>1</sup>, Philippe Ciais<sup>1</sup>, Philippe Bousquet<sup>1</sup>, Michel Ramonet<sup>1</sup>, Yi Yin<sup>1</sup>, Yves Balkanski<sup>1</sup>,  
4 Anne Cozic<sup>1</sup>, Marc Delmotte<sup>1</sup>, Nikolaos Evangeliou<sup>2</sup>, Nuggehalli K. Indira<sup>3</sup>, Robin  
5 Locatelli<sup>1a</sup>, Shushi Peng<sup>4</sup>, Shilong Piao<sup>4</sup>, Marielle Saunois<sup>1</sup>, Panangady S. Swathi<sup>3</sup>, Rong  
6 Wang<sup>1</sup>, Camille Yver-Kwok<sup>1</sup>, Yogesh K. Tiwari<sup>5</sup>, Lingxi Zhou<sup>6</sup>

7

8

9

10 Affiliations:

11 <sup>1</sup>Laboratoire des Sciences du Climat et de l'Environnement, LSCE-IPSL (CEA-CNRS-  
12 UVSQ), Université Paris-Saclay, 91191 Gif-sur-Yvette, France

13 <sup>2</sup>Norwegian Institute for Air Research (NILU), Department of Atmospheric and Climate  
14 Research (ATMOS), Kjeller, Norway

15 <sup>3</sup>CSIR Fourth Paradigm Institute (formerly CSIR Centre for Mathematical Modelling and  
16 Computer Simulation), NAL Belur Campus, Bengaluru 560 037, India

17 <sup>4</sup>Sino-French Institute for Earth System Science, College of Urban and Environmental  
18 Sciences, Peking University, Beijing 100871, China

19 <sup>5</sup>Centre for Climate Change Research, Indian Institute of Tropical Meteorology, Pune, India

20 <sup>6</sup>Chinese Academy of Meteorological Sciences (CAMS), China Meteorological  
21 Administration (CMA), Beijing, China

22

23 *Correspondence to:* X. Lin ([xin.lin@lsce.ipsl.fr](mailto:xin.lin@lsce.ipsl.fr))

24

25 <sup>a</sup> Now at: AXA Global P&C, Paris, France



## 26 Abstract

27 The increasing availability of atmospheric measurements of greenhouse gases (GHGs) from  
28 surface stations can improve the retrieval of their fluxes at higher spatial and temporal  
29 resolutions by inversions, provided that transport models are able to properly represent the  
30 variability of concentrations observed at different stations. South and East Asia (SEA) is a  
31 region with large and very uncertain emissions of carbon dioxide (CO<sub>2</sub>) and methane (CH<sub>4</sub>),  
32 the most potent anthropogenic GHGs. Monitoring networks have expanded greatly during the  
33 past decade in this region, which should contribute to reducing uncertainties in estimates of  
34 regional GHG budgets. In this study, we simulate concentrations of CH<sub>4</sub> and CO<sub>2</sub> using a  
35 zoomed version (abbreviated as 'ZAs') of the global chemistry transport model LMDzINCA,  
36 which has fine horizontal resolutions of ~0.66° in longitude and ~0.51° in latitude over SEA  
37 and coarser resolutions elsewhere. The concentrations of CH<sub>4</sub> and CO<sub>2</sub> simulated from ZAs  
38 are compared to those from the same model but with standard model grids of 2.50° in  
39 longitude and 1.27° in latitude (abbreviated as 'STs'), both prescribed with the same natural  
40 and anthropogenic fluxes. Model performance is evaluated for each model version at multi-  
41 annual, seasonal, synoptic and diurnal scales, against a unique observation dataset including  
42 39 global and regional stations over SEA and around the world. Results show that ZAs  
43 improve the overall representation of CH<sub>4</sub> annual gradients between stations in SEA, with  
44 reduction of RMSE by 16–20% compared to STs. The model improvement mainly results  
45 from reduction in representation error at finer horizontal resolutions and thus better  
46 characterization of the CH<sub>4</sub> concentration gradients related to scatterly distributed emission  
47 sources. However, the performance of ZAs at a specific station as compared to STs is more  
48 sensitive to errors in meteorological forcings and surface fluxes, especially when short-term  
49 variabilities or stations close to source regions are examined. This emphasizes importance of  
50 accurate a priori CH<sub>4</sub> surface fluxes in high resolution transport modelling and inverse studies,  
51 particularly regarding locations and magnitudes of emission hotspots. Model performance for  
52 CO<sub>2</sub> suggests that the CO<sub>2</sub> surface fluxes have not been prescribed with sufficient accuracy  
53 and resolution, especially the spatio-temporally varying carbon exchange between land  
54 surface and atmosphere. Besides, representation of the CH<sub>4</sub> and CO<sub>2</sub> short-term variabilities  
55 is also limited by model's ability to simulate boundary layer mixing and mesoscale transport  
56 in complex terrains, emphasizing the need to improve sub-grid physical parameterizations in  
57 addition to refinement of model resolutions.

## 58 **1 Introduction**

59 Despite attrition in the global network of greenhouse gas (GHG) monitoring stations  
60 (Houweling et al., 2012), new surface stations have been installed since the late 2000s in the  
61 northern industrialized continents such as Europe (e.g., Aalto et al., 2007; Biraud et al., 2000;  
62 Haszpra, 1995; Levin et al., 1995; Lopez et al., 2015; Popa et al., 2010), North America (e.g.,  
63 Bakwin et al., 1998; Dlugokencky et al., 1995; Miles et al., 2012), and Northeast Asia (e.g.,  
64 Fang et al., 2014; Sasakawa et al., 2010; Wada et al., 2011; Winderlich et al., 2010). In  
65 particular, the number of continuous monitoring stations over land has increased (e.g., Aalto  
66 et al., 2007; Bakwin et al., 1998; Lopez et al., 2015; Winderlich et al., 2010) given that more  
67 stable and precise instruments are available (e.g., Yver Kwok et al., 2015). These  
68 observations can be assimilated in inversion frameworks that combine them with a chemistry  
69 transport model and prior knowledge of fluxes to optimize GHG sources and sinks (Berchet  
70 et al., 2015; Bergamaschi et al., 2010, 2015, Bousquet et al., 2000, 2006; Bruhwiler et al.,  
71 2014; Gurney et al., 2002; Peters et al., 2010; Rödenbeck et al., 2003). Given the increasing  
72 observation availability, GHG budgets are expected to be retrieved at finer spatial and  
73 temporal resolutions by atmospheric inversions if the atmospheric GHG variability can be  
74 properly modeled at these scales. A first step of any source optimization is to evaluate the  
75 ability of chemistry transport models to represent the variabilities of GHG concentrations, as  
76 transport errors are recognized as one of the main uncertainties in atmospheric inversions  
77 (Locatelli et al., 2013).

78 Many studies have investigated regional and local variations of atmospheric GHG  
79 concentrations using atmospheric chemistry transport models, with spatial resolutions ranging  
80 100–300 km for global models (e.g., Chen and Prinn, 2005; Feng et al., 2011; Law et al.,  
81 1996; Patra et al., 2009a, 2009b) and 10–100 km for regional models (e.g., Aalto et al., 2006;  
82 Chevillard et al., 2002; Geels et al., 2004; Wang et al., 2007). Model intercomparison  
83 experiments showed that the atmospheric transport models with higher horizontal resolutions  
84 are more capable of capturing the observed short-term variability at continental sites (Geels et  
85 al., 2007; Law et al., 2008; Maksyutov et al., 2008; Patra et al., 2008; Saeki et al., 2013), due  
86 to reduction of representation errors (point measured versus gridbox-averaged modeled  
87 concentrations), improved model transport, and more detailed description of surface fluxes  
88 and topography (Patra et al., 2008). However, a higher horizontal model resolution also

89 demands high-quality meteorological forcings and prescribed surface fluxes as boundary  
90 conditions (Locatelli et al., 2015a).

91 Two main approaches have been deployed, in an Eulerian modeling context, to address the  
92 need for high-resolution transport modeling of long-lived GHGs. The first approach is to  
93 define a high-resolution grid mesh in a limited spatial domain of interest, and to nest it within  
94 a global model with varying degrees of sophistication to get boundary conditions for the  
95 GHGs advected inside/outside the regional domain (Bergamaschi et al., 2005, 2010; Krol et  
96 al., 2005; Peters et al., 2004). The second approach is to stretch the grid of a global model  
97 over a specific region (the so-called ‘zooming’) while maintaining all parameterizations  
98 consistent (Hourdin et al., 2006). For the former approach, several nested high-resolution  
99 zooms can be embedded into the same model (Krol et al., 2005) to focus on different regions.  
100 The ‘zooming’ approach has the advantage to avoid the nesting problems (e.g., tracers  
101 discontinuity, transport parameterization inconsistency) at the boundaries between a global  
102 and a regional model. In this study, we use the zooming capability of the LMDz model  
103 (Hourdin et al., 2006).

104 South and East Asia (hereafter ‘SEA’) has been the largest anthropogenic GHG emitting  
105 region since the mid 2000s due to its rapid socioeconomic development (Boden et al., 2015;  
106 Olivier et al., 2015; Le Quéré et al., 2015; Tian et al., 2016). Compared to Europe and North  
107 America where sources and sinks of GHGs are partly constrained by atmospheric  
108 observational networks, the quantification of regional GHG fluxes over SEA from  
109 atmospheric inversions remains uncertain because of the low density of surface observations  
110 (e.g., Patra et al., 2013; Swathi et al., 2013; Thompson et al., 2014, 2016). During the past  
111 decade, a number of new surface stations have been deployed (e.g., Fang et al., 2016, 2014;  
112 Ganesan et al., 2013; Lin et al., 2015; Tiwari and Kumar, 2012), which have the potential to  
113 provide new and useful constraints on estimates of GHG fluxes in this region. However,  
114 modeling GHG concentrations at these stations is challenging since they are often located in  
115 complex terrains (e.g. coasts or mountains) or close to large local sources of multiple origins.  
116 To fully take advantage of the new surface observations in SEA, forward modeling studies  
117 based on high-resolution transport models are needed to evaluate the ability of the inversion  
118 framework to assimilate such new observations.

119 In this study, we apply the chemistry transport model LMDzINCA (Folberth et al., 2006;  
120 Hauglustaine et al., 2004; Hourdin et al., 2006; Szopa et al., 2013) zoomed down to a  
121 horizontal resolution of ~50km over SEA to simulate the variations of CH<sub>4</sub> and CO<sub>2</sub> during  
122 the period 2006–2013. The model performance is evaluated against observations from [39](#)  
123 [global and regional](#) stations [inside and outside](#) the zoomed region. The variability of the  
124 observed or simulated concentrations at each station is decomposed for evaluation at different  
125 temporal scales, namely: the annual mean gradients between stations, the seasonal cycle, the  
126 synoptic variability and the diurnal cycle. For comparison, a non-zoomed [standard](#) version of  
127 the same transport model is also run with the same set of surface fluxes and the same vertical  
128 pressure levels, in order to estimate the improvement brought by the zoomed configuration.  
129 The detailed description of the observations and the chemistry transport model is presented in  
130 Section 2, together with the prescribed CH<sub>4</sub> and CO<sub>2</sub> surface fluxes that force the simulations,  
131 as well as the metrics used to quantify the model performance. An evaluation of the  
132 simulations performed is presented and discussed in Section 3, showing capabilities of the  
133 transport model to represent the annual gradients between stations, and the seasonal, synoptic,  
134 and diurnal variations. Conclusions and implications drawn from this study are given in  
135 Section 4.

## 136 **2 Data and Methods**

### 137 **2.1 Model description**

#### 138 2.1.1 LMDzINCA

139 The LMDzINCA model couples a general circulation model developed at the Laboratoire de  
140 Météorologie Dynamique (LMD; Hourdin et al., 2006), and a global chemistry and aerosol  
141 model INteractions between Chemistry and Aerosols (INCA; Folberth et al., 2006;  
142 Hauglustaine et al., 2004). A more recent description of LMDzINCA is presented in Szopa et  
143 al. (2013). To simulate CH<sub>4</sub> and CO<sub>2</sub> concentrations, we run a [standard](#) version of the model  
144 with a horizontal resolution of 2.5° (i.e., 144 model grids) in longitude and 1.27° (i.e., 142  
145 model grids) in latitude (hereafter this version is abbreviated as ‘[STs](#)’) and a zoomed version  
146 with the same number of grid boxes, but a resolution of ~0.66° in longitude and ~0.51° in  
147 latitude in a region of 50–130°E and 0–55°N centered over India and China (hereafter this  
148 version is abbreviated as ‘[ZAs](#)’) (Figure 1; see also Wang et al., 2014, 2016). It means that, in

149 terms of the surface area, a gridcell from STs roughly contains 9 grid-cells from ZAs within  
150 the zoomed region. Both model versions are run with 19 and 39 sigma-pressure layers, thus  
151 rendering four combinations of horizontal and vertical resolutions (i.e., ST19, ZA19, ST39,  
152 ZA39). Vertical diffusion and deep convection are parameterized following the schemes of  
153 Louis (1979) and Tiedtke (1989), respectively. The simulated horizontal wind vectors ( $u$  and  
154  $v$ ) are nudged towards the 6-hourly European Center for Medium Range Weather Forecast  
155 (ECMWF) reanalysis dataset (ERA-I) in order to simulate the observed large scale advection  
156 (Hourdin and Issartel, 2000).

157 The atmospheric concentrations of hydroxyl radicals (OH), the main sink of atmospheric CH<sub>4</sub>,  
158 are produced from a simulation at a horizontal resolution of 3.75° in longitude (i.e., 96 model  
159 grids) and 1.9° in latitude (i.e., 95 model grids) with the full INCA tropospheric  
160 photochemistry scheme (Folberth et al., 2006; Hauglustaine et al., 2004, 2014). The OH  
161 fields are climatological monthly data, and are regridded to the standard and zoomed model  
162 grids, respectively. It should be noted that the spatiotemporal distributions of the OH  
163 concentrations have large uncertainties and vary greatly among different chemical transport  
164 models, therefore the choice of the OH fields may affect the evaluation for CH<sub>4</sub> (especially in  
165 terms of the annual gradients between stations and the seasonal cycles). In this study, as we  
166 focus more on the improvement of performance gained from refinement of the model  
167 resolution rather than model-observation misfits and model bias in CH<sub>4</sub> growth rates, the  
168 influences of OH variations on model improvement are assumed to be very small given that  
169 the OH fields for both ZAs and STs are regridded from a lower model resolution and thus  
170 don't show much difference between the two model versions.

171 The CH<sub>4</sub> and CO<sub>2</sub> concentrations are simulated over the period 2000–2013 with both STs and  
172 ZAs. The first six years (2000–2005) of the simulations are considered as model spin-up,  
173 thus we only compared the simulated CH<sub>4</sub> and CO<sub>2</sub> concentrations with observations during  
174 2006–2013. The initial CH<sub>4</sub> concentration field is defined based on the optimized initial state  
175 from a CH<sub>4</sub> inversion that assimilates observations from 50+ global background stations over  
176 the period 2006–2012 (Locatelli, 2014; Locatelli et al., 2015c). The optimized initial CH<sub>4</sub>  
177 concentration field for the year 2006 is rescaled to the levels of the year 2000 and used as the  
178 initial state in our simulations. The time step of model outputs is hourly.

## 179 2.1.2 Prescribed CH<sub>4</sub> and CO<sub>2</sub> surface fluxes

180 The prescribed CH<sub>4</sub> and CO<sub>2</sub> surface fluxes used as model inputs are presented in Table 1.  
181 We simulate the CH<sub>4</sub> concentration fields using a combination of the following datasets: (1)  
182 the interannually varying anthropogenic emissions obtained from the Emission Database for  
183 Global Atmospheric Research (EDGAR) v4.2 FT2010 product (<http://edgar.jrc.ec.europa.eu>),  
184 including emissions from rice cultivation with the seasonal variations based on Matthews et  
185 al. (1991) imposed to the original yearly data; (2) climatological wetland emissions based on  
186 the scheme developed by Kaplan et al. (2006); (3) interannually and seasonally varying  
187 biomass burning emissions from Global Fire Emissions Database (GFED) v4.1 product  
188 (Randerson et al., 2012; Van Der Werf et al., 2017; <http://www.globalfiredata.org/>), (4)  
189 climatological termite emissions (Sanderson, 1996), (5) climatological ocean emissions  
190 (Lambert and Schmidt, 1993), and (6) climatological soil uptake (Ridgwell et al., 1999). Note  
191 that for anthropogenic emissions from sectors other than rice cultivation, the seasonal  
192 variations are much smaller, and monthly sector-specific dataset is currently not available for  
193 the whole study period. Therefore we do not consider seasonal variations in CH<sub>4</sub> emissions  
194 from those sectors. Based on these emission fields, the global CH<sub>4</sub> emissions in 2010 are 550  
195 TgCH<sub>4</sub>/yr, and 194 TgCH<sub>4</sub>/yr over the zoomed region. For the years over which CH<sub>4</sub>  
196 anthropogenic emissions (namely, the years 2011–2013) were not available from the data  
197 sources when the simulations were performed, we use emissions for the year 2010.

198 The prescribed CO<sub>2</sub> fluxes used to simulate the concentration fields are based on the  
199 following datasets: (1) three variants (hourly, daily, and monthly means) of interannually  
200 varying fossil fuel emissions produced by the Institut für Energiewirtschaft und Rationelle  
201 Energieanwendung (IER), Universität Stuttgart on the basis of EDGARv4.2 product  
202 (hereafter IER-EDGAR, <http://carbones.ier.uni-stuttgart.de/wms/index.html>) (Pregger et al.,  
203 2007); (2) interannually and seasonally varying biomass burning emission from GFEDv4.1  
204 ([Randerson et al., 2012; Van Der Werf et al., 2017; http://www.globalfiredata.org/](http://www.globalfiredata.org/)); (3)  
205 interannually and hourly varying terrestrial biospheric fluxes produced from outputs of the  
206 Organizing Carbon and Hydrology in Dynamic Ecosystem (ORCHIDEE) model; and (4)  
207 interannually and seasonally varying air-sea CO<sub>2</sub> gas exchange maps developed by NOAA's  
208 Pacific Marine Environmental Laboratory (PMEL) and Atlantic Oceanographic and  
209 Meteorological Laboratory (AOML) groups (Park et al., 2010). Here ORCHIDEE runs with  
210 the trunk version r1882 (source code available at

211 <https://forge.ipsl.jussieu.fr/orchidee/browser/trunk#ORCHIDEE> with the revision number of  
212 r1882), using the same simulation protocol as the SG3 simulation in MsTMIP project  
213 (Huntzinger et al., 2013). The climate forcing data are obtained from CRUNCEP v5.3.2,  
214 while the yearly land use maps, soil map and other forcing data (e.g., monthly CO<sub>2</sub>  
215 concentrations) are as described in Wei et al. (2014). The sum of global net CO<sub>2</sub> surface  
216 fluxes in 2010 are 6.9 PgC/yr, and 3.9 PgC/yr over the zoomed region. For the CO<sub>2</sub> fossil fuel  
217 emissions, the IER-EDGAR product is only available until 2009. To generate the emission  
218 maps for the years 2010–2013, we scaled the emission spatial distribution in 2009 using the  
219 global totals for these years based on the EDGARv4.2FT2010 datasets. The detailed  
220 information for each surface flux is listed in Table 1.

## 221 **2.2 Atmospheric CH<sub>4</sub> and CO<sub>2</sub> observations**

222 The simulated CH<sub>4</sub> and CO<sub>2</sub> concentrations are evaluated against observations from 20 flask  
223 and 13 continuous surface stations within and around the zoomed region (Figure 1), operated  
224 by different programs and organizations (Table 2). The stations where flask observations are  
225 published (12 stations) mainly belong to the cooperative program organized by the NOAA  
226 Earth System Research Laboratory (NOAA/ESRL, available at  
227 [ftp://aftp.cmdl.noaa.gov/data/trace\\_gases/](ftp://aftp.cmdl.noaa.gov/data/trace_gases/)). We also use flask observations from stations  
228 operated by China Meteorological Administration (CMA, China) (the JIN, LIN and LON  
229 stations, see also Fang et al., 2014), Commonwealth Scientific and Research Organization  
230 (CSIRO, Australia) (the CRI station, Bhattacharya et al., 2009, available at  
231 <http://ds.data.jma.go.jp/gmd/wdcgg/>), Indian Institute of Tropical Meteorology (IITM, India)  
232 (the SNG station, see also Tiwari et al., 2014), and stations from the Indo-French cooperative  
233 research program (the HLE, PON and PBL stations, Lin et al., 2015; Swathi et al., 2013). All  
234 the CH<sub>4</sub> (CO<sub>2</sub>) flask measurements are reported on or linked to the NOAA2004  
235 (WMOX2007) calibration scale, which guarantees comparability between stations in terms of  
236 annual means.

237 The continuous CH<sub>4</sub> and CO<sub>2</sub> measurements are obtained from 13 stations operated by Korea  
238 Meteorological Administration (KMA, Korea) (the AMY and GSN stations), Aichi Air  
239 Environment Division (AAED, Japan) (the MKW station), Japan Meteorological Agency  
240 (JMA) (the MNM, RYO and YON stations), National Institute for Environmental Studies  
241 (NIES, Japan) (the COI and HAT stations), Agency for Meteorology, Climatology and

242 Geophysics (BMKG, Indonesia) and Swiss Federal Laboratoires for Materials Testing and  
243 Research (Empa, Switzerland) (the BKT station). These datasets are available from the World  
244 Data Center for Greenhouse Gases (WDCGG, <http://ds.data.jma.go.jp/gmd/wdogg/>). Besides,  
245 continuous CH<sub>4</sub> and CO<sub>2</sub> measurements are also available from HLE and PON that have been  
246 maintained by the Indo-French cooperative research program between LSCE in France and  
247 IIA and CSIR4PI in India (Table 2). All the continuous CH<sub>4</sub> (CO<sub>2</sub>) measurements used in this  
248 study are reported on or traceable to the NOAA2004 (WMOX2007) scale except AMY, COI  
249 and HAT. The CO<sub>2</sub> continuous measurements at COI are reported on the NIES95 scale,  
250 which is 0.10 to 0.14 ppm lower than WMO in a range between 355 and 385 ppm (Machida  
251 et al., 2009). The CH<sub>4</sub> continuous measurements at COI and HAT are reported on the NIES  
252 scale, with a conversion factor to WMO scale of 0.9973 (JMA and WMO, 2014). For AMY,  
253 the CH<sub>4</sub> measurements over most of the study period are reported on the KRISS scale but  
254 they are not traceable to the WMO scale (JMA and WMO, 2014); therefore, we discarded  
255 this station from the subsequent analyses of the CH<sub>4</sub> annual gradients between stations. Note  
256 that most of the stations where continuous observations are available are located on the east  
257 part of the zoomed region, with the exception of HLE, PON and BKT. The stations used in  
258 this study span a large range of geographic locations (marine, coastal, mountain or  
259 continental) with polluted and non-polluted environments. Both flask and continuous  
260 measurements are used to evaluate the model's ability in representing the annual gradient  
261 between stations, the seasonal cycle and the synoptic variability for CH<sub>4</sub> and CO<sub>2</sub>. The  
262 continuous measurements are also used to analyze the diurnal cycle for these two gases.

263 To evaluate the model performance with regards to vertical transport, we also use  
264 observations of the CO<sub>2</sub> vertical profiles from passenger aircraft from the Comprehensive  
265 Observation Network for TRace gases by AirLiner (CONTRAIL) project (Machida et al.,  
266 2008, <http://www.cger.nies.go.jp/contrail/index.html>). This dataset provides high-frequency  
267 CO<sub>2</sub> measurements made by on-board continuous CO<sub>2</sub> measuring equipments (CMEs) during  
268 commercial flights between Japan and other Asian countries. The CONTRAIL data are  
269 reported on the NIES95 scale, which is 0.10 to 0.14 ppm lower than WMO in a range  
270 between 355 and 385 ppm (Machida et al., 2009). In this study, we select from the  
271 CONTRAIL dataset all the CO<sub>2</sub> vertical profiles over SEA during the ascending and  
272 descending flights for the period 2006–2011, which provided 1808 vertical profiles over a  
273 total of 32 airports (Figure S1 and S2).



## 274 2.3 Sampling methods and data processing

275 The model outputs are sampled at the nearest gridpoint and vertical level to each station for  
276 both [STs](#) and [ZAs](#). For flask stations, the model outputs are extracted at the exact hour when  
277 each flask sample was taken. For continuous stations below 1000 m.a.s.l., since both [STs](#) and  
278 [ZAs](#) cannot reproduce accurately the nighttime CH<sub>4</sub> and CO<sub>2</sub> accumulation near the ground  
279 as in most transport models (Geels et al., 2007), only afternoon (12:00–15:00 LST) data are  
280 retained for further analyses of the annual gradients, the seasonal cycle and the synoptic  
281 variability. For continuous stations above 1000 m.a.s.l. (only HLE in this study), nighttime  
282 (00:00–3:00 LST) data are retained, to avoid sampling local air masses advected by upslope  
283 winds from nearby valleys. During daytime, the local valley ascendances and the complex  
284 terrain mesoscale circulations cannot be captured by a global transport model.

285 The curve-fitting routine (CCGvu) developed by NOAA Climate Monitoring and Diagnostic  
286 Laboratory (NOAA/CMDL) is applied to the modelled and observed CH<sub>4</sub> and CO<sub>2</sub> time  
287 series to extract the annual means, monthly smoothed seasonal cycles and synoptic variations  
288 (Thoning et al., 1989). For each station, a smoothed function is fitted to the observed or  
289 modelled time series, which consists of a first-order polynomial for the growth rate, two  
290 harmonics for the annual cycle (Levin et al., 2002; Ramonet et al., 2002), and a low-pass  
291 filter with 80 and 667 days as short-term and long-term cutoff values, respectively (Bakwin et  
292 al., 1998). The annual means and the mean seasonal cycle are calculated from the smoothed  
293 curve and harmonics, while the synoptic variations are defined as the residuals between the  
294 original data and the smoothed fitting curve. Note that we have excluded the observations  
295 lying beyond three standard deviations of the residuals around the fitting curve, which are  
296 likely to be outliers that are influenced by local fluxes. More detailed descriptions about the  
297 curve-fitting procedures and the set-up of parameters can be found in Section 2.3 of Lin et al.  
298 (2015).

299 For the CO<sub>2</sub> vertical profiles from the CONTRAIL passenger aircraft programme, since CO<sub>2</sub>  
300 data have been continuously taken every 10 seconds by the onboard CMEs, we average the  
301 observed and corresponding simulated CO<sub>2</sub> time series into altitude bins of 1km from the  
302 surface to the upper troposphere. We also divide the whole study area into four major  
303 subregions for which we group all available CONTRAIL CO<sub>2</sub> profiles (Figure S1), namely  
304 East Asia (EAS), the Indian sub-continent (IND), Northern Southeast Asia (NSA) and

305 Southern Southeast Asia (SSA). Given that there are model-observation discrepancies in CO<sub>2</sub>  
306 growth rates as well as misfits of absolute CO<sub>2</sub> concentrations, the observed and simulated  
307 CONTRAIL time series have been detrended before comparisons of the vertical gradients. To  
308 this end, over each subregion, we detrend for each altitude bin the observed and simulated  
309 CO<sub>2</sub> time series, by applying the respective linear trend fit to the observed and simulated CO<sub>2</sub>  
310 time series of the altitude bin 3–4 km. This altitude bin is thus chosen as reference due to  
311 greater data availability compared to other altitudes, and because this level is outside the  
312 boundary layer where aircraft CO<sub>2</sub> data are more variable and influenced by local sources  
313 (e.g. airports and nearby cities). The detrended CO<sub>2</sub> (denoted as  $\Delta\text{CO}_2$ ) referenced to the 3-4  
314 km altitude are seasonally averaged for each altitude bin and each subregion, and the  
315 resulting vertical profiles of  $\Delta\text{CO}_2$  are compared between simulations and observations.

## 316 2.4 Metrics

317 In order to evaluate the model performance to represent observations at different time scales  
318 (annual, seasonal, synoptic, diurnal), following Cadule et al. (2010), we define a series of  
319 metrics and corresponding statistics for each time scale. All the metrics, defined below, are  
320 calculated for both observed and simulated CH<sub>4</sub> (CO<sub>2</sub>) time series between 2006 and 2013.

### 321 2.4.1 Annual gradients between stations

322 As inversions use gradients to optimize surface fluxes, it is important to have a metric based  
323 upon cross-site gradients. We take Hanle in India (HLE – 78.96°N, 32.78°E, 4517 m a.s.l.,  
324 Figure 1, Table 2) as a reference and calculate the mean annual gradients by subtracting CH<sub>4</sub>  
325 (CO<sub>2</sub>) at HLE from those of other stations. HLE is a remote station in the free troposphere  
326 within SEA and is located far from any important source/sink areas for both CH<sub>4</sub> and CO<sub>2</sub>.  
327 These characteristics make HLE an appropriate reference to calculate the gradients between  
328 stations. Concentration gradients to HLE are calculated for both observations and model  
329 simulations using the corresponding smoothed curves fitted with the CCGvu routine (see  
330 Section 2.3). The ability of ZAs and STs to represent the observed CH<sub>4</sub> (CO<sub>2</sub>) annual  
331 gradients across all the available stations is quantified by the mean bias (MB, Eq. 1) and the  
332 root-mean-square deviation (RMSE, Eq. 2). In Eq. 1 and Eq. 2,  $m_i$  and  $o_i$  indicate  
333 respectively the modelled and observed CH<sub>4</sub> (CO<sub>2</sub>) mean annual gradient relative to HLE for  
334 a station  $i$ .

335 
$$MB = \frac{\sum_{i=1}^N (m_i - o_i)}{N} \quad (1)$$

336 
$$RMSE = \sqrt{\frac{\sum_{i=1}^N (m_i - o_i)^2}{N}} \quad (2)$$

337 2.4.2 Seasonal cycle

338 Two metrics of the model ability to reproduce the observed CH<sub>4</sub> (CO<sub>2</sub>) seasonal cycle are  
 339 considered, the phase and the amplitude. For each station, the seasonal phase is evaluated by  
 340 the Pearson correlation between the observed and simulated harmonics extracted from the  
 341 original time series, whereas the seasonal cycle amplitude is evaluated by the ratio of the  
 342 modelled to the observed seasonal peak-to-peak amplitudes based on the harmonics ( $A_m/A_o$ ).

343 2.4.3 Synoptic variability

344 | For each station, the performance of ZAs and STs to represent the phase (timing) of the  
 345 synoptic variability is evaluated by the Pearson correlation coefficient between the modelled  
 346 and observed synoptic deviations (residuals) around the corresponding smoothed fitting curve  
 347 (see Section 2.3), whereas the performance for the amplitude of the synoptic variability is  
 348 quantified by the ratio of standard deviations of the residual concentration variability between  
 349 the model and observations (i.e., Normalized Standard Deviation, NSD, Eq. 3). Further, the  
 350 overall ability of a model to represent the synoptic variability of CH<sub>4</sub> (CO<sub>2</sub>) at a station is  
 351 quantified by the RMSE (Eq. 4), a metric that can be represented with the Pearson correlation  
 352 and the NSD in a Taylor diagram (Taylor, 2001). In Eq. 3 and Eq. 4,  $m_j$  ( $o_j$ ) indicates the  
 353 modelled (observed) synoptic event  $j$ , whereas  $\bar{m}$  ( $\bar{o}$ ) indicates the arithmetic mean of all the  
 354 modelled (observed) synoptic events over the study period. Note that for the flask  
 355 measurements,  $j$  corresponds to the time when a flask sample was taken, whereas for the  
 356 continuous measurements,  $j$  corresponds to the early morning (00:00–03:00LST, for  
 357 mountain stations) or afternoon (12:00–15:00LST, for coastal or island stations) period of  
 358 each sampling day.

359 
$$NSD = \frac{\sqrt{\frac{\sum_{j=1}^N (m_j - \bar{m})^2}{N}}}{\sqrt{\frac{\sum_{j=1}^N (o_j - \bar{o})^2}{N}}} \quad (3)$$

360 
$$RMSE = \sqrt{\frac{\sum_{j=1}^N (m_j - o_j)^2}{N}} \quad (4)$$

361 2.4.4 Diurnal cycle

362 For each station, the model's ability to reproduce the mean CH<sub>4</sub> (CO<sub>2</sub>) diurnal cycle phase in  
 363 a month is evaluated by the correlation of the hourly mean composite modelled and observed  
 364 values, whereas model performance on the diurnal cycle amplitude is evaluated by the ratio  
 365 of the modelled to the observed peak-to-peak amplitudes ( $A_m/A_o$ ). For each station, daily  
 366 means are subtracted from the raw data to remove any influence of interannual, seasonal or  
 367 even synoptic variations.

368 **3 Results and discussions**

369 **3.1 Annual gradients**

370 3.1.1 CH<sub>4</sub> annual gradients

371 The annual mean gradient between a station and the HLE reference station relates to the time  
 372 integral of transport of sources/sinks within the regional footprint area of the station on top of  
 373 the background gradient caused by remote sources. For CH<sub>4</sub>, Figure 2a,b shows the  
 374 scatterplot of the simulated and observed mean annual gradients to HLE for all stations. In  
 375 general, all the four model versions capture the observed CH<sub>4</sub> gradients with reference to  
 376 HLE, and the simulated gradients roughly distribute around the identity line (Figure 2a,b).  
 377 Compared to standard versions (STs), the zoom versions (ZAs) better represent the CH<sub>4</sub>  
 378 gradients for stations within the zoomed region (closed circles in Figure 2a,b), with RMSE  
 379 decreasing by 20% and 16% for 19- and 39-layer models (Figure 2a,b and Table S1a). Note  
 380 that increasing vertical resolution does not much impact the overall model performance, but  
 381 the combination with the zoomed grid (i.e. ZA39) may inflate the model-observation misfits  
 382 at a few stations with strong sources nearby (e.g. TAP and UUM in Table S2a). The better

383 performance of ZAs within the zoomed region is also found for different seasons (Figure S3).  
384 Outside the zoomed region (open circles in Figure 2a,b), the performance of ZAs does not  
385 significantly deteriorate despite the coarser resolution.

386 When looking into the model performance for different station types, ZAs generally better  
387 capture the gradients at coastal and continental stations within the zoomed region, given the  
388 substantial reduction of RMSE compared to STs (Table S1). For example, significant model  
389 improvement is found at Shangdianzi (SDZ – 117.12°E, 40.65°N, 293m a.s.l.) and  
390 Pondicherry (PON – 79.86°E, 12.01°N, 30m a.s.l.) (Figure 2a,b), each having an average bias  
391 reduction of 28.1 (73.0%) and 30.3 (94.7%) ppb respectively compared to STs for the 39-  
392 layer model (Table S2). This improvement mainly results from reduction in representation  
393 error with higher model horizontal resolutions in the zoomed region, through better  
394 description of surface fluxes and/or transport around the stations. Particularly, given the  
395 presence of large CH<sub>4</sub> emission hotspots within the zoomed region (Figure S4), ZAs makes  
396 the simulated CH<sub>4</sub> fields more heterogeneous around emission hotspots (e.g., North China in  
397 Figure S5), having the potential to better represent stations nearby on an annual basis if the  
398 surface fluxes are prescribed with sufficient accuracy (see Figure S6 for SDZ).

399 However, finer resolutions may enhance model-data misfits due to inaccurate meteorological  
400 forcings and/or surface flux maps. For example, for the coastal station Tae-ahn Peninsula  
401 (TAP – 126.13°E, 36.73°N, 21m a.s.l.) with significant emission sources nearby (Figure S6),  
402 both ZAs and STs overestimate the observed CH<sub>4</sub> gradients by  $\geq +15$  ppb, and ZA39 perform  
403 even worse than other versions (Table S2). The poor model performance at TAP suggests that  
404 the prescribed emission sources are probably overestimated within the station's footprint area  
405 (also see the marine station GSN, Figure S6), and higher model resolutions (whether in  
406 horizontal or in vertical) tend to inflate the model-observation misfits in this case. Besides, as  
407 stated in several previous studies (Geels et al., 2007; Law et al., 2008; Patra et al., 2008), for  
408 a station located in a complex terrain (e.g. coastal or mountain sites), the selection of an  
409 appropriate gridpoint and/or model level to represent an observation is challenging. In this  
410 study we sample the gridpoint and model level nearest to the location of the station, which  
411 may not be the best representation of data sampling selection strategy (e.g. marine sector at  
412 coastal stations or strong winds) and could contribute to the model-observation misfits.

### 413 3.1.2 CO<sub>2</sub> annual gradients

414 Both ZAs and STs can generally capture the CO<sub>2</sub> annual gradients between stations, although  
415 not as well as for CH<sub>4</sub> (Figure 2c,d). In contrast with CH<sub>4</sub>, ZAs does not significantly  
416 improve representation of CO<sub>2</sub> gradients for stations within the zoomed region, with the mean  
417 bias and RMSE close to those of STs (Table S1b). At a few stations (e.g., TAP), ZAs even  
418 degrade model performance (Figure S8, Table S2b), possibly related to misrepresentation of  
419 CO<sub>2</sub> sources in the prescribed surface fluxes and transport effects. Again increasing model  
420 vertical resolution does not much impact the overall model performance.

421 With finer horizontal resolution, the model improvement to represent the annual gradients is  
422 more apparent for CH<sub>4</sub> than for CO<sub>2</sub>. One of the reasons may point towards the quality of  
423 CO<sub>2</sub> surface fluxes, especially natural ones. They are spatially more diffuse than those of CH<sub>4</sub>,  
424 and temporally more variable in response to weather changes (Parazoo et al., 2008; Wang et  
425 al., 2007). Therefore, the regional variations of net ecosystem exchange (NEE) not captured  
426 by the terrestrial ecosystem model (e.g. ORCHIDEE in this paper) may explain the worse  
427 model performance on the CO<sub>2</sub> annual gradients compared to CH<sub>4</sub>, and less apparent model  
428 improvement. Further, the spatial resolution of the prescribed surface flux may also account  
429 for the difference in model improvement between CO<sub>2</sub> and CH<sub>4</sub> (e.g. the spatial resolution of  
430 anthropogenic emissions is 1° for CO<sub>2</sub> and 0.1° for CH<sub>4</sub>). Therefore, with current setup of  
431 surface fluxes (Table 1), ZAs is more likely to resolve the spatial heterogeneity of CH<sub>4</sub> fields,  
432 and its improvement over STs is more apparent than that for CO<sub>2</sub>.

## 433 3.2 Seasonal cycles

### 434 3.2.1 CH<sub>4</sub> seasonal cycles

435 The model performance for the seasonal cycle depends on quality of seasonal surface fluxes,  
436 atmospheric transport, and chemistry (for CH<sub>4</sub> only). For CH<sub>4</sub>, both ZAs and STs very well  
437 capture the seasonal phases at most stations within the zoomed region (Figure 3a), and model  
438 resolutions (in both horizontal and vertical) do not significantly impact the simulated timing  
439 of seasonal maximum and minimum. The seasonal phases at Plateau Assy (KZM – 77.87°E,  
440 43.25°N, 2524m a.s.l.), Waliguan (WLG – 100.90°E, 36.28°N, 3890m a.s.l.) and Ulaan Uul  
441 (UUM – 111.10°E, 44.45°N, 1012m a.s.l.) are not well represented, probably related to  
442 unresolved seasonally varying sources around these stations. The sensitivity test simulations

443 prescribed with wetland emissions from ORCHIDEE outputs show much better model-  
444 observation agreement in seasonal phases (Figure S9). For stations outside the zoomed region,  
445 the performance of ZAs is not degraded despite the coarser horizontal resolutions (Figure  
446 S10).

447 With respect to the seasonal amplitude, the performance of STs and ZAs shows significant  
448 difference at stations influenced by large emission sources. For example, the seasonal  
449 amplitudes of AMY and TAP are strongly overestimated by STs ( $A_m/A_o = 2.99$  and  
450  $A_m/A_o = 5.11$  for the 39-layer model; Figure 3a), while ZAs substantially decrease the  
451 simulated amplitudes at these two stations with improved model-observation agreement  
452 ( $A_m/A_o = 2.24$  and  $A_m/A_o = 2.80$  for the 39-layer model; Figure 3a). However, at SDZ the  
453 seasonal amplitude is even more exaggerated by ZAs, especially when higher vertical  
454 resolution is applied ( $A_m/A_o = 1.70$  and  $A_m/A_o = 2.03$  for ST39 and ZA39; Figure 3a). The two  
455 contrasting cases suggest that increasing horizontal resolution does not necessarily better  
456 represent CH<sub>4</sub> seasonal cycle, and model improvement/degradation depends on other factors  
457 such as accuracy of the temporal and spatial variations of prescribed fluxes, OH fields and  
458 meteorological forcings. Besides, as it is found for annual CH<sub>4</sub> gradients, we note that the  
459 simulated seasonal amplitudes at stations in East Asia (AMY, TAP, GSN and SDZ) are  
460 consistently higher than the observed ones (Figure 3a), implying that the prescribed CH<sub>4</sub>  
461 emissions are probably overestimated in this region.

### 462 3.2.2 CO<sub>2</sub> seasonal cycles

463 The CO<sub>2</sub> seasonal cycle mainly represents the seasonal cycle of NEE from ORCHIDEE  
464 convoluted with atmospheric transport. Figure 3b illustrates that both ZAs and STs well  
465 capture the CO<sub>2</sub> seasonal phases at most stations, and a high correlation (Pearson correlation  
466  $R > 0.8$ ) between the simulated and observed CO<sub>2</sub> harmonics is found for 14 out of 20 stations  
467 within the zoomed region. However, the simulated onset of CO<sub>2</sub> uptake in spring or timing of  
468 the seasonal minima tend to be earlier than observations. This shift in phase can be as large  
469 as >1 month for several stations (e.g. HLE, JIN and PON in Figure 3b), yet cannot be reduced  
470 by solely refining model resolutions. At BKT in western Indonesia, the shape of the CO<sub>2</sub>

471 seasonality is not well captured ( $R=0.27$  and  $R=0.30$  for ST39 and ZA39; Figure 3b). Given  
472 that representation of the  $\text{CH}_4$  seasonal phase at BKT is very good ( $R=0.97$  for ST39 and  
473 ZA39; Figure 3a), the unsatisfactory model performance for  $\text{CO}_2$  suggests inaccurate  
474 seasonal variations in the prescribed surface fluxes such as NEE and/or fire emissions. As for  
475  $\text{CH}_4$ , the performance of ZAs is not degraded outside the zoomed region despite the coarser  
476 horizontal resolutions (Figure S11).

477 With respect to the  $\text{CO}_2$  seasonal amplitude, 10 out of 20 stations within the zoomed region  
478 are underestimated by more than 20%, most of which are mountain and continental stations  
479 (Figure 3b). The underestimation of  $\text{CO}_2$  seasonal amplitudes at these stations is probably due  
480 to the underestimated carbon uptake in northern mid-latitudes by ORCHIDEE, which is the  
481 case for most land surface models currently available (Peng et al., 2015). Another reason may  
482 be related to the misrepresentation of  $\text{CO}_2$  seasonal rectifier effect (Denning et al., 1995),  
483 which means that the covariance between carbon exchange (through photosynthesis and  
484 respiration) and vertical mixing may not be well captured in our simulations even with finer  
485 model resolutions.

### 486 **3.3 Synoptic variability**

#### 487 3.3.1 $\text{CH}_4$ synoptic variability

488 The day-to-day variability of  $\text{CH}_4$  and  $\text{CO}_2$  residuals are influenced by the regional  
489 distribution of fluxes and atmospheric transport at the synoptic scale. For  $\text{CH}_4$ , as shown in  
490 Figure 4a, both STs and ZAs fairly well capture the phases of synoptic variability at most  
491 stations within the zoomed region, with 15 out of 18 stations showing model-observation  
492 correlation  $r>0.3$ . Increasing horizontal resolution can more or less impact model  
493 performance, yet the direction of change is station-dependent. In general, ZAs improve  
494 correlation in phases for most marine and coastal stations compared to STs (e.g., CRI and  
495 HAT; Figure 4a), while degradation in model performance is mostly found for mountain and  
496 continental stations (e.g. KZM and SDZ; Figure 4a). With increased horizontal resolution,  
497 better characterization of the phases would require accurate representation of short-term  
498 variability in both meteorological forcings and emission sources at fine scales. This presents  
499 great challenges on data quality of boundary conditions, especially for mountain stations  
500 located in complex terrains or continental stations surrounded by highly heterogeneous yet  
501 uncertain emission sources.



502 Regarding the amplitudes of CH<sub>4</sub> synoptic variability, 12 out of 18 stations have NSDs within  
503 the range of 0.6–1.5, and ZAs generally give higher NSD values than STs for most of these  
504 stations (Figure 4b). For stations with NSDs>1.5, ZAs tend to simulate smaller amplitudes  
505 and slightly improve model performance (e.g., GSN, HLE and SDZ; Figure 4b). One  
506 exception is UUM. Given the presence of a wrong emission hotspot near the station in the  
507 EDGARv4.2FT2010 dataset, ZAs greatly inflate the model-observation misfits (Figure S13).  
508 The sensitivity test simulations prescribed with an improved data version EDGARv4.3.2  
509 show much better agreement with observations, although the simulated amplitudes are still  
510 too high. Besides, it is interesting to note that stations in East Asia generally have NSDs>1.5  
511 (e.g., GSN, TAP, SDZ, and UUM; Figure 4b), again suggesting overestimation of the  
512 prescribed CH<sub>4</sub> emissions in this region.

### 513 3.3.2 CO<sub>2</sub> synoptic variability

514 For CO<sub>2</sub>, as shown in Figure 4c and 4d, 12 out of 20 stations within the zoomed region have  
515 model-observation correlation  $r>0.3$ , whereas 14 out of 20 stations have NSDs within the  
516 range of 0.5–1.5. With finer model resolution, significant model improvement (whether  
517 regarding phases or amplitudes of CO<sub>2</sub> synoptic variability) is mostly found at marine, coastal  
518 and continental stations (e.g., AMY, DSI, and SDZ; Figure 4c,d); for mountain stations, on  
519 the contrary, phase correlation is not improved and representation of amplitudes is even  
520 degraded (e.g. HLE, LLN and WLG; Figure 4c,d). As mentioned above for CH<sub>4</sub> synoptic  
521 variability, the model degradation at mountain stations may arise from errors in mesoscale  
522 meteorology and regional distribution of sources/sinks over complex terrains, probably as  
523 well as unresolved vertical processes.

524 When we examine model performance for CO<sub>2</sub> versus CH<sub>4</sub> by stations, there are stations at  
525 which phases of synoptic variability are satisfactorily captured for CH<sub>4</sub> but not for CO<sub>2</sub> (e.g.,  
526 BKT, PBL, PON; Figure 4a,c). At PON, a tropical station on the southeast coast of India, the  
527 simulated CO<sub>2</sub> synoptic variability is even out of phase with observations all year around and  
528 during different seasons (Figure S15; Table S3). The poor model performance should be  
529 largely attributed to the imperfect prescribed CO<sub>2</sub> surface fluxes. As noted by several  
530 previous studies (e.g., Patra et al., 2008), CO<sub>2</sub> fluxes with sufficient accuracy and resolution  
531 are indispensable for realistic simulation of CO<sub>2</sub> synoptic variability. In this study, the daily  
532 to hourly NEE variability does not seem to be well represented in ORCHIDEE, especially in

533 the tropics. Further, for stations influenced by large fire emissions (e.g., BKT), using the  
534 monthly averaged biomass burning emissions may not be able to realistically simulate CO<sub>2</sub>  
535 synoptic variability due to episodic biomass burning events. Besides, the prescribed CO<sub>2</sub>  
536 ocean fluxes have a rather coarse spatial resolution (4°×5°), which may additionally account  
537 for the poor model performance, especially for marine and coastal stations.

### 538 **3.4 Diurnal cycle**

#### 539 3.4.1 CH<sub>4</sub> diurnal cycle

540 The diurnal cycles of trace gases are mainly controlled by the co-variations between local  
541 surface fluxes and atmospheric transport. To illustrate model performance on diurnal cycles,  
542 we take a few stations with continuous measurements as examples. For CH<sub>4</sub>, as shown in  
543 Figure 5a, the mean diurnal cycles can be reasonably well represented at the marine/coastal  
544 stations GSN and PON for the specific study periods (also see Table S4), although monthly  
545 fluxes are used to prescribe the models. Compared to STs, the diurnal cycles simulated by  
546 ZAs agree much better with observations (Figure 5a), possibly due to more realistic  
547 representation of coastal topography, land-sea breeze, and/or source distribution at finer grids.  
548 However, there are also periods during which the CH<sub>4</sub> diurnal cycles are not satisfactorily  
549 represented by both model versions, or model performance is degraded with higher  
550 horizontal/vertical resolutions (Table S4). The model-observation mismatch may be  
551 explained by the following reasons. First, the prescribed monthly surface fluxes are probably  
552 not adequate to resolve the short-term variability at stations strongly influenced by local and  
553 regional sources, especially during the seasons when emissions from wetlands and rice  
554 paddies are active and temporally variable with temperature and moisture. Second, the sub-  
555 grid scale parameterizations in the current model we used are not able to realistically simulate  
556 the diurnal cycles of boundary layer mixing. Recently new physical parameterizations have  
557 been implemented in LMDz to better simulate vertical diffusion and mesoscale mixing by  
558 thermal plumes in the boundary layer (Hourdin et al., 2002; Rio et al., 2008), which can  
559 significantly improve simulation of the daily peak values during nighttime and thus diurnal  
560 cycles of tracer concentrations (Locatelli et al., 2015b).

561 Representation of the CH<sub>4</sub> diurnal cycle at mountain stations can be even more complicated,  
562 given that the mesoscale atmospheric transports such as mountain-valley circulations and  
563 terrain-induced up-down slope circulations cannot be resolved in global transport models

564 (Griffiths et al., 2014; Pérez-Landa et al., 2007; Pillai et al., 2011). At BKT, a mountain  
565 station located on an altitude of 869 m a.s.l., the CH<sub>4</sub> diurnal cycle is not reasonably  
566 represented when model outputs are sampled at the levels corresponding to this altitude (Level  
567 3 and Level 4 for 19-layer and 39-layer models). The simulated CH<sub>4</sub> diurnal cycles sampled  
568 at a lower model level (Level 2 for both 19-layer and 39-layer models) agree much better  
569 with the observed ones (Figure 5a). This suggests that the current model in use is not able to  
570 resolve mesoscale circulations in complex terrains, even with the zoomed grids (~50 km over  
571 the focal area) and 39 model layers.

### 572 3.4.2 CO<sub>2</sub> diurnal cycle

573 For CO<sub>2</sub>, as shown in Figure 5b, the simulated diurnal cycles at GSN and PON correlate  
574 fairly well with the observed ones for their specific study periods (also see Table S5). The  
575 amplitudes of diurnal cycles are greatly underestimated, although this can be more or less  
576 improved with finer horizontal resolutions (Figure 5b). As for CH<sub>4</sub>, the model-observation  
577 discrepancies mainly result from underestimated NEE diurnal cycles from ORCHIDEE  
578 and/or unresolved processes in the planetary boundary layer. Particularly, neither ZAs nor  
579 STs are able to adequately capture the CO<sub>2</sub> diurnal rectifier effect (Denning et al., 1996). For  
580 stations strongly influenced by local fossil fuel emissions, underestimation of the amplitudes  
581 may be additionally attributed to fine-scale sources not resolved at current horizontal  
582 resolutions. This is the case for PON, a coastal station 8 km north of the city of Pondicherry  
583 in India with a population of around 750,000 (Lin et al., 2015), where the amplitudes of  
584 diurnal cycles are underestimated for both CO<sub>2</sub> and CH<sub>4</sub> (Figure 5a,b). Again at BKT, as  
585 noted for CH<sub>4</sub>, a better model-observation agreement is found for the CO<sub>2</sub> diurnal cycle when  
586 model outputs are sampled at the surface layer rather than the one corresponding to the  
587 station altitude (Figure 5b). Note that even the simulated diurnal cycles at the surface level  
588 are smaller compared to the observed ones by ~50%, suggesting that the diurnal variations of  
589 both NEE fluxes and terrain-induced circulations are probably not satisfactorily represented  
590 in the current simulations.

### 591 3.5 Evaluation against the CONTRAIL CO<sub>2</sub> vertical profiles

592 Figure 6 shows the simulated and observed CO<sub>2</sub> vertical profiles averaged for different  
593 seasons and over different regions. Over East Asia (EAS; Figure 6a and Figure S1), both ZAs  
594 and STs reasonably reproduce the shape of the observed CO<sub>2</sub> vertical profiles above 2 km,

595 | while below 2 km the magnitude of  $\Delta\text{CO}_2$  is significantly underestimated by up to 5 ppm.  
596 | The simulated  $\text{CO}_2$  vertical gradients between planetary boundary layer (BL) and free  
597 | troposphere (FT) are lower than the observations by 2–3 ppm during winter (Figure 7a). The  
598 | model-observation discrepancies are possibly due to stronger vertical mixing in LMDz  
599 | (Locatelli et al., 2015a; Patra et al., 2011) as well as flux uncertainty. Note that as most  
600 | samples (79%) are taken over the Narita International Airport (NRT) and Chubu Centrair  
601 | International Airport (NGO) in Japan located outside the zoomed region (Figure S1), STs  
602 | slightly better capture the BL-FT gradients than ZAs.

603 | Over the Indian sub-continent (IND, Figure 6b), there is large underestimation of the  
604 | magnitude of  $\Delta\text{CO}_2$  near the surface by up to 8 ppm during April–June (AMJ), July–  
605 | September (JAS) and October–December (OND). Accordingly, the BL-FT gradients are also  
606 | underestimated by up to 3–4ppm for these periods (Figure 7b). The model-observation  
607 | discrepancies are probably due to vertical mixing processes not realistically simulated in the  
608 | current model (including deep convection), as well as the imperfect representation of  $\text{CO}_2$   
609 | surface fluxes strongly influenced by the Indian monsoon system.

610 | The  $\text{CO}_2$  vertical profiles over Southeast Asia (including Northern Southeast Asia (NSA) and  
611 | Southern Southeast Asia (SSA)) are generally well reproduced (Figure 6c,d). However, both  
612 | ZAs and STs fail to reproduce the BL-FT gradient of  $\sim 3$  ppm in April for NSA (Figure 7c).  
613 | Apart from errors due to vertical transport and/or prescribed NEE, inaccurate estimates of  
614 | biomass burning emissions could also contribute to this model-observation mismatch.

615 | Overall, the  $\text{CO}_2$  vertical profiles in free troposphere are well simulated by both STs and ZAs  
616 | over SEA, while significant underestimation of the BL-FT gradients is found for East Asia  
617 | and the Indian sub-continent. The model-observation mismatch is due to misrepresentation of  
618 | both vertical transport and prescribed surface fluxes, and can not be significantly reduced by  
619 | solely refining the horizontal/vertical resolution, as shown by the very similar  $\text{CO}_2$  vertical  
620 | profiles simulated from ZAs and STs. New physical parameterization as shown in Locatelli et  
621 | al., (2015a) should be implemented in the model to assess its potential to improve simulation  
622 | of the vertical profiles of trace gases (especially the BL-FT gradients).

## 623 4 Conclusions and implications

624 In this study, we assess the capability of a global transport model (LMDzINCA) to simulate  
625 CH<sub>4</sub> and CO<sub>2</sub> variabilities over South and East Asia (SEA). Simulations have been performed  
626 with configurations of different horizontal (standard (STs) versus Asian zoom (ZAs)) and  
627 vertical (19 versus 39) resolutions. Model performance to represent trace gas variabilities is  
628 evaluated for each model version at multi-annual, seasonal, synoptic and diurnal scales,  
629 against flask and continuous measurements from a unique dataset of 39 global and regional  
630 stations inside and outside the zoomed region. The evaluation at multiple temporal scales and  
631 comparisons between different model resolutions and trace gases have informed us of both  
632 advantages and challenges relating to high resolution transport modelling. Main conclusions  
633 and implications for possible model improvement and inverse modeling are summarized as  
634 follows.

635 First, ZAs improve the overall representation of CH<sub>4</sub> annual gradients between stations in  
636 SEA, with reduction of RMSE by 16–20% compared to STs. The model improvement mainly  
637 results from reduction in representation error with finer horizontal resolutions over SEA,  
638 through better characterization of CH<sub>4</sub> surface fluxes, transport, and/or topography around  
639 stations. Particularly, the scatterly distributed CH<sub>4</sub> emission sources (especially emission  
640 hotspots) can be more precisely defined with the Asian zoom grids, which makes the  
641 simulated concentration fields more heterogeneous, having the potential to improve  
642 representation of stations nearby on an annual basis.

643 However, as the model resolution increases, the simulated CH<sub>4</sub> concentration fields are more  
644 sensitive to possible errors in boundary conditions. Thus the performance of ZAs at a specific  
645 station as compared to STs depends on the accuracy and data quality of meteorological  
646 forcings and/or surface fluxes, especially when we examine short-term variabilities (synoptic  
647 and diurnal variations) or stations influenced by significant emission sources around. One  
648 example is UUM, at which ZAs even greatly degrade representation of synoptic variability  
649 due to presence of a wrong emission hotspot near the station in the EDGARv4.2FT2010  
650 dataset. A sensitivity test prescribed with the improved emission dataset EDGARv4.3.2 show  
651 much better agreement with observations. This emphasizes importance of accurate a priori  
652 CH<sub>4</sub> surface fluxes in high resolution transport modelling and inversions, particularly  
653 regarding locations and magnitudes of emission hotspots. Any unrealistic emission hotspot

654 close to a station (as shown for UUM) should be corrected before inversions, otherwise the  
655 inverted surface fluxes are likely to be strongly biased. Moreover, as current bottom-up  
656 estimates of CH<sub>4</sub> sources and sinks still suffer from large uncertainties at fine scales, caution  
657 should be taken when one attempts to assimilate observations not realistically simulated by  
658 the high resolution transport model. These observations should be either removed from  
659 inversions or allocated with large uncertainties.

660 With respect to CO<sub>2</sub>, model performance and the limited model improvement with finer grids  
661 suggest that the CO<sub>2</sub> surface fluxes have not been prescribed with sufficient accuracy and  
662 resolution. One major component is NEE simulated from the terrestrial ecosystem model  
663 ORCHIDEE. For example, the smaller CO<sub>2</sub> seasonal amplitudes simulated at most inland  
664 stations in SEA mainly result from underestimated carbon uptake in northern mid-latitudes by  
665 ORCHIDEE, while the misrepresentation of synoptic and diurnal variabilities (especially for  
666 tropical stations like BKT and PON) is related to the inability of ORCHIDEE to satisfactorily  
667 capture sub-monthly to daily profiles of NEE. More efforts should be made to improve  
668 simulation of carbon exchange between land surface and atmosphere at various spatial and  
669 temporal scales.

670 Furthermore, apart from data quality of the prescribed surface fluxes, representation of the  
671 CH<sub>4</sub> and CO<sub>2</sub> short-term variabilities is also limited by model's ability to simulate boundary  
672 layer mixing and mesoscale transport in complex terrains. The recent implementation of new  
673 sub-grid physical parameterizations in LMDz is able to significantly improve simulation of  
674 the daily maximum during nighttime and thus diurnal cycles of tracer concentrations  
675 (Locatelli et al., 2015b). To fully take advantage of high-frequency CH<sub>4</sub> or CO<sub>2</sub> observations  
676 at stations close to source regions, it is highly recommended to implement the new boundary  
677 layer physics in the current transport model, in addition to refinement of model horizontal  
678 and vertical resolutions. The current transport model with old planetary boundary physics is  
679 not capable to capture diurnal variations at continental or mountain stations, therefore only  
680 observations that are well represented should be selected and kept for inversions (e.g.  
681 afternoon measurements for continental stations and nighttime measurements for mountain  
682 stations).

683 Lastly, the model-observation comparisons at multiple temporal scales can give us  
684 information about the magnitude of sources and sinks in the studied region. For example, at

685 GSN, TAP and SDZ, all of which located in East and Northeast Asia, the CH<sub>4</sub> annual  
686 gradients as well as the amplitudes of seasonal and synoptic variability are consistently  
687 overestimated, suggesting overestimation of CH<sub>4</sub> emissions in East Asia. Therefore  
688 atmospheric inversions that assimilate information from these stations are expected to  
689 decrease emissions in East Asia, which agree with several recent global or regional studies  
690 from independent inventories (e.g., Peng et al., 2016) or inverse modeling (Bergamaschi et al.,  
691 2013; Bruhwiler et al., 2014; Thompson et al., 2015). Further studies are needed in the future  
692 to estimate CH<sub>4</sub> budgets in SEA by utilizing high resolution transport models that are capable  
693 to represent regional networks of atmospheric observations.

## 694 **Acknowledgement**

695 This study was initiated within the framework of CaFICA-CEFIPRA project (2809-1). X. Lin  
696 acknowledges the PhD funding support from AIRBUS Defense & Space. P. Ciais thanks the  
697 ERC SyG project IMBALANCE-P ‘Effects of Phosphorus Limitations on Life, Earth System  
698 and Society’ Grant agreement (no. 610028). N. Evangeliou acknowledges the Nordic Center  
699 of Excellence eSTICC project (eScience Tools for Investigating Climate Change in northern  
700 high latitudes) funded by Nordforsk (no. 57001). We acknowledge the WDCGG for  
701 providing the archives of surface station observations for CO<sub>2</sub> and CH<sub>4</sub>. We thank the  
702 following networks or institutes for the efforts on surface GHG measurements and their  
703 access: NOAA/ESRL, Aichi, BMKG, CMA, CSIR4PI, CSIRO, Empa, ESSO/NIOT, IIA,  
704 IITM, JMA, KMA, LSCE, NIER, NIES, PU and Saitama. We also thank Dr. T. Machida  
705 from NIES for providing CO<sub>2</sub> measurements from the CONTRAIL project. Finally, we  
706 would like to thank F. Marabelle and his team at LSCE, and the CURIE (TGCC) platform for  
707 the computing support.

708



709 **References**

- 710 Aalto, T., Hatakka, J., Karstens, U., Aurela, M., Thum, T. and Lohila, A.: Modeling  
711 atmospheric CO<sub>2</sub> concentration profiles and fluxes above sloping terrain at a boreal site,  
712 *Atmos. Chem. Phys.*, 6(2), 303–314, doi:10.5194/acp-6-303-2006, 2006.
- 713 Aalto, T., Hatakka, J. and Lallo, M.: Tropospheric methane in northern Finland: seasonal  
714 variations, transport patterns and correlations with other trace gases, *Tellus B*, 59(2), 251–259,  
715 doi:10.1111/j.1600-0889.2007.00248.x, 2007.
- 716 Bakwin, P. S., Tans, P. P., Hurst, D. F. and Zhao, C.: Measurements of carbon dioxide on  
717 very tall towers: results of the NOAA/CMDL program, *Tellus B*, 50(5), 401–415,  
718 doi:10.1034/j.1600-0889.1998.t01-4-00001.x, 1998.
- 719 Berchet, A., Pison, I., Chevallier, F., Paris, J.-D., Bousquet, P., Bonne, J.-L., Arshinov, M. Y.,  
720 Belan, B. D., Cressot, C., Davydov, D. K., Dlugokencky, E. J., Fofonov, A. V., Galanin, A.,  
721 Lavrič, J., Machida, T., Parker, R., Sasakawa, M., Spahni, R., Stocker, B. D. and Winderlich,  
722 J.: Natural and anthropogenic methane fluxes in Eurasia: a mesoscale quantification by  
723 generalized atmospheric inversion, *Biogeosciences*, 12(18), 5393–5414, doi:10.5194/bg-12-  
724 5393-2015, 2015.
- 725 Bergamaschi, P., Corazza, M., Karstens, U., Athanassiadou, M., Thompson, R. L., Pison, I.,  
726 Manning, A. J., Bousquet, P., Segers, A., Vermeulen, A. T., Janssens-Maenhout, G., Schmidt,  
727 M., Ramonet, M., Meinhardt, F., Aalto, T., Haszpra, L., Moncrieff, J., Popa, M. E., Lowry,  
728 D., Steinbacher, M., Jordan, A., O’Doherty, S., Piacentino, S. and Dlugokencky, E.: Top-  
729 down estimates of European CH<sub>4</sub> and N<sub>2</sub>O emissions based on four different inverse models,  
730 *Atmos. Chem. Phys.*, 15(2), 715–736, doi:10.5194/acp-15-715-2015, 2015.
- 731 Bergamaschi, P., Houweling, S., Segers, A., Krol, M., Frankenberg, C., Scheepmaker, R. A.,  
732 Dlugokencky, E., Wofsy, S. C., Kort, E. A., Sweeney, C., Schuck, T., Brenninkmeijer, C.,  
733 Chen, H., Beck, V. and Gerbig, C.: Atmospheric CH<sub>4</sub> in the first decade of the 21st century:  
734 Inverse modeling analysis using SCIAMACHY satellite retrievals and NOAA surface  
735 measurements, *J. Geophys. Res. Atmos.*, 118(13), 7350–7369, doi:10.1002/jgrd.50480, 2013.
- 736 Bergamaschi, P., Krol, M., Dentener, F., Vermeulen, A., Meinhardt, F., Graul, R., Ramonet,  
737 M., Peters, W. and Dlugokencky, E. J.: Inverse modelling of national and European CH<sub>4</sub>  
738 emissions using the atmospheric zoom model TM5, *Atmos. Chem. Phys.*, 5(9), 2431–2460,  
739 doi:10.5194/acp-5-2431-2005, 2005.
- 740 Bergamaschi, P., Krol, M., Meirink, J. F., Dentener, F., Segers, A., van Aardenne, J., Monni,  
741 S., Vermeulen, A. T., Schmidt, M., Ramonet, M., Yver, C., Meinhardt, F., Nisbet, E. G.,  
742 Fisher, R. E., O’Doherty, S. and Dlugokencky, E. J.: Inverse modeling of European CH<sub>4</sub>  
743 emissions 2001–2006, *J. Geophys. Res. Atmos.*, 115(D22), D22309,  
744 doi:10.1029/2010JD014180, 2010.
- 745 Bhattacharya, S. K., Borole, D. V., Francey, R. J., Allison, C. E., Steele, L. P., Krummel, P.,  
746 Langenfelds, R., Masarie, K. A., Tiwari, Y. K. and Patra, P. K.: Trace gases and CO<sub>2</sub> isotope  
747 records from Cabo de Rama, India, *Curr. Sci.*, 97(9), 1336–1344, 2009.
- 748 Biraud, S., Ciais, P., Ramonet, M., Simmonds, P., Kazan, V., Monfray, P., O’Doherty, S.,  
749 Spain, T. G. and Jennings, S. G.: European greenhouse gas emissions estimated from  
750 continuous atmospheric measurements and <sup>222</sup>Rn at Mace Head, Ireland, *J. Geophys. Res.*  
751 *Atmos.*, 105(D1), 1351–1366, doi:10.1029/1999JD900821, 2000.

752 Boden, T. A., Marland, G. and Andres, R. J.: Global, Regional, and National Fossil-Fuel CO<sub>2</sub>  
753 Emissions, Oak Ridge, Tenn., USA., 2015.

754 Bousquet, P., Ciais, P., Miller, J. B., Dlugokencky, E. J., Hauglustaine, D. A., Prigent, C.,  
755 Van der Werf, G. R., Peylin, P., Brunke, E.-G., Carouge, C., Langenfelds, R. L., Lathiere, J.,  
756 Papa, F., Ramonet, M., Schmidt, M., Steele, L. P., Tyler, S. C. and White, J.: Contribution of  
757 anthropogenic and natural sources to atmospheric methane variability, *Nature*, 443(7110),  
758 439–443 [online] Available from: <http://dx.doi.org/10.1038/nature05132>, 2006.

759 Bousquet, P., Peylin, P., Ciais, P., Le Quéré, C., Friedlingstein, P. and Tans, P. P.: Regional  
760 changes in carbon dioxide fluxes of land and oceans since 1980, *Science* (80-. ), 290(5495),  
761 1342–1346 [online] Available from:  
762 <http://science.sciencemag.org/content/290/5495/1342.abstract>, 2000.

763 Bruhwiler, L., Dlugokencky, E., Masarie, K., Ishizawa, M., Andrews, A., Miller, J., Sweeney,  
764 C., Tans, P. and Worthy, D.: CarbonTracker-CH<sub>4</sub>: an assimilation system for estimating  
765 emissions of atmospheric methane, *Atmos. Chem. Phys.*, 14(16), 8269–8293,  
766 doi:10.5194/acp-14-8269-2014, 2014.

767 Cadule, P., Friedlingstein, P., Bopp, L., Sitch, S., Jones, C. D., Ciais, P., Piao, S. L. and  
768 Peylin, P.: Benchmarking coupled climate-carbon models against long-term atmospheric CO<sub>2</sub>  
769 measurements, *Global Biogeochem. Cycles*, 24(2), GB2016, doi:10.1029/2009GB003556,  
770 2010.

771 Chen, Y.-H. and Prinn, R. G.: Atmospheric modeling of high- and low-frequency methane  
772 observations: Importance of interannually varying transport, *J. Geophys. Res. Atmos.*,  
773 110(D10), D10303, doi:10.1029/2004JD005542, 2005.

774 Chevillard, A., Karstens, U. T. E., Ciais, P., Lafont, S. and Heimann, M.: Simulation of  
775 atmospheric CO<sub>2</sub> over Europe and western Siberia using the regional scale model REMO,  
776 *Tellus B*, 54(5), 872–894, doi:10.1034/j.1600-0889.2002.01340.x, 2002.

777 Denning, A. S., Fung, I. Y. and Randall, D.: Latitudinal gradient of atmospheric CO<sub>2</sub> due to  
778 seasonal exchange with land biota, *Nature*, 376(6537), 240–243, doi:10.1038/376240a0, 1995.

779 Denning, A. S., Randall, D. A., Collatz, G. J. and Sellers, P. J.: Simulations of terrestrial  
780 carbon metabolism and atmospheric CO<sub>2</sub> in a general circulation model, *Tellus B*, 48(4),  
781 543–567, doi:10.1034/j.1600-0889.1996.t01-1-00010.x, 1996.

782 Dlugokencky, E. J., Steele, L. P., Lang, P. M. and Masarie, K. A.: Atmospheric methane at  
783 Mauna Loa and Barrow observatories: Presentation and analysis of in situ measurements, *J.*  
784 *Geophys. Res. Atmos.*, 100(D11), 23103–23113, doi:10.1029/95JD02460, 1995.

785 Fang, S., Tans, P. P., Dong, F., Zhou, H. and Luan, T.: Characteristics of atmospheric CO<sub>2</sub>  
786 and CH<sub>4</sub> at the Shangdianzi regional background station in China, *Atmos. Environ.*, 131, 1–8,  
787 doi:<http://dx.doi.org/10.1016/j.atmosenv.2016.01.044>, 2016.

788 Fang, S. X., Zhou, L. X., Tans, P. P., Ciais, P., Steinbacher, M., Xu, L. and Luan, T.: In situ  
789 measurement of atmospheric CO<sub>2</sub> at the four WMO/GAW stations in China, *Atmos. Chem.*  
790 *Phys.*, 14(5), 2541–2554, doi:10.5194/acp-14-2541-2014, 2014.

791 Feng, L., Palmer, P. I., Yang, Y., Yantosca, R. M., Kawa, S. R., Paris, J.-D., Matsueda, H.  
792 and Machida, T.: Evaluating a 3-D transport model of atmospheric CO<sub>2</sub> using ground-based,  
793 aircraft, and space-borne data, *Atmos. Chem. Phys.*, 11(6), 2789–2803, doi:10.5194/acp-11-  
794 2789-2011, 2011.

795 Folberth, G. A., Hauglustaine, D. A., Lathière, J. and Brocheton, F.: Interactive chemistry in  
796 the Laboratoire de Météorologie Dynamique general circulation model: model description  
797 and impact analysis of biogenic hydrocarbons on tropospheric chemistry, *Atmos. Chem.*  
798 *Phys.*, 6(8), 2273–2319, doi:10.5194/acp-6-2273-2006, 2006.

799 Ganesan, A. L., Chatterjee, A., Prinn, R. G., Harth, C. M., Salameh, P. K., Manning, A. J.,  
800 Hall, B. D., Mühle, J., Meredith, L. K., Weiss, R. F., O’Doherty, S. and Young, D.: The  
801 variability of methane, nitrous oxide and sulfur hexafluoride in Northeast India, *Atmos.*  
802 *Chem. Phys.*, 13(21), 10633–10644, doi:10.5194/acp-13-10633-2013, 2013.

803 Geels, C., Doney, S. C., Dargaville, R., Brandt, J. and Christensen, J. H.: Investigating the  
804 sources of synoptic variability in atmospheric CO<sub>2</sub> measurements over the Northern  
805 Hemisphere continents: a regional model study, *Tellus B*, 56(1), 35–50, doi:10.1111/j.1600-  
806 0889.2004.00084.x, 2004.

807 Geels, C., Gloor, M., Ciais, P., Bousquet, P., Peylin, P., Vermeulen, A. T., Dargaville, R.,  
808 Aalto, T., Brandt, J., Christensen, J. H., Frohn, L. M., Haszpra, L., Karstens, U., Rödenbeck,  
809 C., Ramonet, M., Carboni, G. and Santaguida, R.: Comparing atmospheric transport models  
810 for future regional inversions over Europe &ndash; Part 1: mapping the atmospheric CO<sub>2</sub>  
811 signals, *Atmos. Chem. Phys.*, 7(13), 3461–3479, doi:10.5194/acp-7-3461-2007, 2007a.

812 Geels, C., Gloor, M., Ciais, P., Bousquet, P., Peylin, P., Vermeulen, A. T., Dargaville, R.,  
813 Aalto, T., Brandt, J., Christensen, J. H., Frohn, L. M., Haszpra, L., Karstens, U., Rödenbeck,  
814 C., Ramonet, M., Carboni, G. and Santaguida, R.: Comparing atmospheric transport models  
815 for future regional inversions over Europe &ndash; Part 1: mapping the atmospheric CO<sub>2</sub>  
816 signals, *Atmos. Chem. Phys.*, 7(13), 3461–3479, doi:10.5194/acp-7-3461-2007, 2007b.

817 Griffiths, A. D., Conen, F., Weingartner, E., Zimmermann, L., Chambers, S. D., Williams, A.  
818 G. and Steinbacher, M.: Surface-to-mountaintop transport characterised by radon  
819 observations at the Jungfraujoch, *Atmos. Chem. Phys.*, 14(23), 12763–12779,  
820 doi:10.5194/acp-14-12763-2014, 2014.

821 Gurney, K. R., Law, R. M., Denning, A. S., Rayner, P. J., Baker, D., Bousquet, P., Bruhwiler,  
822 L., Chen, Y.-H., Ciais, P., Fan, S., Fung, I. Y., Gloor, M., Heimann, M., Higuchi, K., John, J.,  
823 Maki, T., Maksyutov, S., Masarie, K., Peylin, P., Prather, M., Pak, B. C., Randerson, J.,  
824 Sarmiento, J., Taguchi, S., Takahashi, T. and Yuen, C.-W.: Towards robust regional  
825 estimates of CO<sub>2</sub> sources and sinks using atmospheric transport models, *Nature*, 415(6872),  
826 626–630 [online] Available from: <http://dx.doi.org/10.1038/415626a>, 2002.

827 Haszpra, L.: Carbon dioxide concentration measurements at a rural site in Hungary, *Tellus B*,  
828 47(1–2), 17–22, doi:10.1034/j.1600-0889.47.issue1.3.x, 1995.

829 Hauglustaine, D. A., Balkanski, Y. and Schulz, M.: A global model simulation of present and  
830 future nitrate aerosols and their direct radiative forcing of climate, *Atmos. Chem. Phys.*,  
831 14(20), 11031–11063, doi:10.5194/acp-14-11031-2014, 2014.

832 Hauglustaine, D. A., Hourdin, F., Jourdain, L., Filiberti, M.-A., Walters, S., Lamarque, J.-F.  
833 and Holland, E. A.: Interactive chemistry in the Laboratoire de Météorologie Dynamique  
834 general circulation model: Description and background tropospheric chemistry evaluation, *J.*  
835 *Geophys. Res. Atmos.*, 109(D4), D04314, doi:10.1029/2003JD003957, 2004.

836 Hourdin, F., Couvreux, F., Menut, L., Hourdin, F., Couvreux, F. and Menut, L.:  
837 Parameterization of the Dry Convective Boundary Layer Based on a Mass Flux  
838 Representation of Thermals, *J. Atmos. Sci.*, 59(6), 1105–1123, doi:10.1175/1520-

- 839 0469(2002)059<1105:POTDCB>2.0.CO;2, 2002.
- 840 Hourdin, F. and Issartel, J.-P.: Sub-surface nuclear tests monitoring through the CTBT Xenon  
841 Network, *Geophys. Res. Lett.*, 27(15), 2245–2248, doi:10.1029/1999GL010909, 2000.
- 842 Hourdin, F., Musat, I., Bony, S., Braconnot, P., Codron, F., Dufresne, J.-L., Fairhead, L.,  
843 Filiberti, M.-A., Friedlingstein, P., Grandpeix, J.-Y., Krinner, G., LeVan, P., Li, Z.-X. and  
844 Lott, F.: The LMDZ4 general circulation model: climate performance and sensitivity to  
845 parametrized physics with emphasis on tropical convection, *Clim. Dyn.*, 27(7–8), 787–813,  
846 doi:10.1007/s00382-006-0158-0, 2006.
- 847 Houweling, S., Badawy, B., Baker, D. F., Basu, S., Belikov, D., Bergamaschi, P., Bousquet,  
848 P., Broquet, G., Butler, T., Canadell, J. G., Chen, J., Chevallier, F., Ciais, P., Collatz, G. J.,  
849 Denning, S., Engelen, R., Enting, I. G., Fischer, M. L., Fraser, A., Gerbig, C., Gloor, M.,  
850 Jacobson, A. R., Jones, D. B. A., Heimann, M., Khalil, A., Kaminski, T., Kasibhatla, P. S.,  
851 Krakauer, N. Y., Krol, M., Maki, T., Maksyutov, S., Manning, A., Meesters, A., Miller, J. B.,  
852 Palmer, P. I., Patra, P., Peters, W., Peylin, P., Poussi, Z., Prather, M. J., Randerson, J. T.,  
853 Röckmann, T., Rödenbeck, C., Sarmiento, J. L., Schimel, D. S., Scholze, M., Schuh, A.,  
854 Suntharalingam, P., Takahashi, T., Turnbull, J., Yurganov, L. and Vermeulen, A.: Iconic  
855 CO<sub>2</sub> Time Series at Risk, *Science* (80-. ), 337(6098), 1038–1040 [online] Available from:  
856 <http://science.sciencemag.org/content/337/6098/1038.2.abstract>, 2012.
- 857 Huntzinger, D. N., Schwalm, C., Michalak, A. M., Schaefer, K., King, A. W., Wei, Y.,  
858 Jacobson, A., Liu, S., Cook, R. B., Post, W. M., Berthier, G., Hayes, D., Huang, M., Ito, A.,  
859 Lei, H., Lu, C., Mao, J., Peng, C. H., Peng, S., Poulter, B., Riccuto, D., Shi, X., Tian, H.,  
860 Wang, W., Zeng, N., Zhao, F. and Zhu, Q.: The North American Carbon Program Multi-  
861 Scale Synthesis and Terrestrial Model Intercomparison Project – Part 1: Overview and  
862 experimental design, *Geosci. Model Dev.*, 6(6), 2121–2133, doi:10.5194/gmd-6-2121-2013,  
863 2013.
- 864 JMA and WMO: WMO WDCGG Data Summary (WDCGG No. 38) Volume IV -  
865 Greenhouse Gases and other Atmospheric Gases. [online] Available from:  
866 <http://ds.data.jma.go.jp/gmd/wdcgg/pub/products/summary/sum38/sum38.pdf>, 2014.
- 867 Kaplan, J. O., Folberth, G. and Hauglustaine, D. A.: Role of methane and biogenic volatile  
868 organic compound sources in late glacial and Holocene fluctuations of atmospheric methane  
869 concentrations, *Global Biogeochem. Cycles*, 20(2), GB2016, doi:10.1029/2005GB002590,  
870 2006.
- 871 Krol, M., Houweling, S., Bregman, B., van den Broek, M., Segers, A., van Velthoven, P.,  
872 Peters, W., Dentener, F. and Bergamaschi, P.: The two-way nested global chemistry-transport  
873 zoom model TM5: algorithm and applications, *Atmos. Chem. Phys.*, 5(2), 417–432,  
874 doi:10.5194/acp-5-417-2005, 2005.
- 875 Lambert, G. and Schmidt, S.: Reevaluation of the oceanic flux of methane: Uncertainties and  
876 long term variations, *Chemosphere*, 26(1–4), 579–589, doi:http://dx.doi.org/10.1016/0045-  
877 6535(93)90443-9, 1993.
- 878 Law, R. M., Peters, W., Rödenbeck, C., Aulagnier, C., Baker, I., Bergmann, D. J., Bousquet,  
879 P., Brandt, J., Bruhwiler, L., Cameron-Smith, P. J., Christensen, J. H., Delage, F., Denning, A.  
880 S., Fan, S., Geels, C., Houweling, S., Imasu, R., Karstens, U., Kawa, S. R., Kleist, J., Krol, M.  
881 C., Lin, S.-J., Lokupitiya, R., Maki, T., Maksyutov, S., Niwa, Y., Onishi, R., Parazoo, N.,  
882 Patra, P. K., Pieterse, G., Rivier, L., Satoh, M., Serrar, S., Taguchi, S., Takigawa, M.,

883 Vautard, R., Vermeulen, A. T. and Zhu, Z.: TransCom model simulations of hourly  
884 atmospheric CO<sub>2</sub>: Experimental overview and diurnal cycle results for 2002, *Global*  
885 *Biogeochem. Cycles*, 22(3), GB3009, doi:10.1029/2007GB003050, 2008.

886 Law, R. M., Rayner, P. J., Denning, A. S., Erickson, D., Fung, I. Y., Heimann, M., Piper, S.  
887 C., Ramonet, M., Taguchi, S., Taylor, J. A., Trudinger, C. M. and Watterson, I. G.:  
888 Variations in modeled atmospheric transport of carbon dioxide and the consequences for CO<sub>2</sub>  
889 inversions, *Global Biogeochem. Cycles*, 10(4), 783–796, doi:10.1029/96GB01892, 1996.

890 Levin, I., Ciais, P., Langenfelds, R., Schmidt, M., Ramonet, M., Sidorov, K., Tchebakova, N.,  
891 Gloor, M., Heimann, M., Schulze, E.-D., Vygodskaya, N. N., Shibistova, O. and Lloyd, J.:  
892 Three years of trace gas observations over the EuroSiberian domain derived from aircraft  
893 sampling — a concerted action, *Tellus B*, 54(5), 696–712, doi:10.1034/j.1600-  
894 0889.2002.01352.x, 2002.

895 Levin, I., Graul, R. and Trivett, N. B. A.: Long-term observations of atmospheric CO<sub>2</sub> and  
896 carbon isotopes at continental sites in Germany, *Tellus B*, 47(1–2), 23–34,  
897 doi:10.1034/j.1600-0889.47.issue1.4.x, 1995.

898 Lin, X., Indira, N. K., Ramonet, M., Delmotte, M., Ciais, P., Bhatt, B. C., Reddy, M. V.,  
899 Angchuk, D., Balakrishnan, S., Jorphail, S., Dorjai, T., Mahey, T. T., Patnaik, S., Begum, M.,  
900 Brenninkmeijer, C., Durairaj, S., Kirubakaran, R., Schmidt, M., Swathi, P. S., Vinithkumar,  
901 N. V., Yver Kwok, C. and Gaur, V. K.: Long-lived atmospheric trace gases measurements in  
902 flask samples from three stations in India, *Atmos. Chem. Phys.*, 15(17), 9819–9849,  
903 doi:10.5194/acp-15-9819-2015, 2015.

904 Locatelli, R.: Estimation des sources et puits de méthane: bilan planétaire et impacts de la  
905 modélisation du transport atmosphérique, Versailles-St Quentin en Yvelines, France. [online]  
906 Available from: <http://www.theses.fr/2014VERS0035>, 2014.

907 Locatelli, R., Bousquet, P., Chevallier, F., Fortems-Cheney, A., Szopa, S., Saunois, M.,  
908 Agusti-Panareda, A., Bergmann, D., Bian, H., Cameron-Smith, P., Chipperfield, M. P., Gloor,  
909 E., Houweling, S., Kawa, S. R., Krol, M., Patra, P. K., Prinn, R. G., Rigby, M., Saito, R. and  
910 Wilson, C.: Impact of transport model errors on the global and regional methane emissions  
911 estimated by inverse modelling, *Atmos. Chem. Phys.*, 13(19), 9917–9937, doi:10.5194/acp-  
912 13-9917-2013, 2013.

913 Locatelli, R., Bousquet, P., Hourdin, F., Saunois, M., Cozic, A., Couvreux, F., Grandpeix, J.-  
914 Y., Lefebvre, M.-P., Rio, C., Bergamaschi, P., Chambers, S. D., Karstens, U., Kazan, V., van  
915 der Laan, S., Meijer, H. A. J., Moncrieff, J., Ramonet, M., Scheeren, H. A., Schlosser, C.,  
916 Schmidt, M., Vermeulen, A. and Williams, A. G.: Atmospheric transport and chemistry of  
917 trace gases in LMDz5B: evaluation and implications for inverse modelling, *Geosci. Model*  
918 *Dev.*, 8(2), 129–150, doi:10.5194/gmd-8-129-2015, 2015a.

919 Locatelli, R., Bousquet, P., Hourdin, F., Saunois, M., Cozic, A., Couvreux, F., Grandpeix, J.-  
920 Y., Lefebvre, M.-P., Rio, C., Bergamaschi, P., Chambers, S. D., Karstens, U., Kazan, V., Van  
921 Der Laan, S., Meijer, H. A. J., Moncrieff, J., Ramonet, M., Scheeren, H. A., Schlosser, C.,  
922 Schmidt, M., Vermeulen, A. and Williams, A. G.: Atmospheric transport and chemistry of  
923 trace gases in LMDz5B: evaluation and implications for inverse modelling, *Geosci. Model*  
924 *Dev.*, 8, 129–150, doi:10.5194/gmd-8-129-2015, 2015b.

925 Locatelli, R., Bousquet, P., Saunois, M., Chevallier, F. and Cressot, C.: Sensitivity of the  
926 recent methane budget to LMDz sub-grid-scale physical parameterizations, *Atmos. Chem.*

- 927 Phys, 15, 9765–9780, doi:10.5194/acp-15-9765-2015, 2015c.
- 928 Lopez, M., Schmidt, M., Ramonet, M., Bonne, J.-L., Colomb, A., Kazan, V., Laj, P. and  
929 Pichon, J.-M.: Three years of semicontinuous greenhouse gas measurements at the Puy de  
930 Dôme station (central France), *Atmos. Meas. Tech.*, 8(9), 3941–3958, doi:10.5194/amt-8-  
931 3941-2015, 2015.
- 932 Louis, J.-F.: A parametric model of vertical eddy fluxes in the atmosphere, *Boundary-Layer*  
933 *Meteorol.*, 17(2), 187–202, doi:10.1007/BF00117978, 1979.
- 934 Machida, T., Katsumata, K., Tohjima, Y., Watai, T. and Mukai, H.: Preparing and  
935 maintaining of CO<sub>2</sub> calibration scale in National Institute for Environmental Studies: NIES  
936 95 CO<sub>2</sub> scale, in Report of the 14th WMO/IAEA Meeting of Experts on Carbon Dioxide  
937 Concentration and Related Tracer Measurement Techniques, edited by T. Laurila, pp. 26–29,  
938 GMO/GAW Report No. 186, Helsinki., 2009.
- 939 Machida, T., Matsueda, H., Sawa, Y., Nakagawa, Y., Hirotsu, K., Kondo, N., Goto, K.,  
940 Nakazawa, T., Ishikawa, K. and Ogawa, T.: Worldwide measurements of atmospheric CO<sub>2</sub>  
941 and other trace gas species using commercial airlines, *J. Atmos. Ocean. Technol.*, 25(10),  
942 1744–1754, doi:10.1175/2008JTECHA1082.1, 2008.
- 943 Maksyutov, S., Patra, P. K., Onishi, R., Saeki, T. and Nakazawa, T.: NIES/FRCGC Global  
944 Atmospheric Tracer Transport Model: Description, validation, and surface sources and sinks  
945 inversion, *J. Earth Simulator*, 9, 3–18, 2008.
- 946 Matthews, E., Fung, I. and Lerner, J.: Methane emission from rice cultivation: Geographic  
947 and seasonal distribution of cultivated areas and emissions, *Global Biogeochem. Cycles*, 5(1),  
948 3–24, doi:10.1029/90GB02311, 1991.
- 949 Miles, N. L., Richardson, S. J., Davis, K. J., Lauvaux, T., Andrews, A. E., West, T. O.,  
950 Bandaru, V. and Crosson, E. R.: Large amplitude spatial and temporal gradients in  
951 atmospheric boundary layer CO<sub>2</sub> mole fractions detected with a tower-based network in the  
952 U.S. upper Midwest, *J. Geophys. Res. Biogeosciences*, 117(G1), n/a-n/a,  
953 doi:10.1029/2011JG001781, 2012.
- 954 Olivier, J. G. J., Janssens-Maenhout, G., Munten, M. and Peters, J. A. H. W.: Trends in  
955 global CO<sub>2</sub> emissions: 2015 Report., 2015.
- 956 Parazoo, N. C., Denning, A. S., Kawa, S. R., Corbin, K. D., Lokupitiya, R. S. and Baker, I. T.:  
957 Mechanisms for synoptic variations of atmospheric CO<sub>2</sub> in North America, South America  
958 and Europe, *Atmos. Chem. Phys.*, 8(23), 7239–7254, doi:10.5194/acp-8-7239-2008, 2008.
- 959 Park, G., Wanninkhof, R. I. F., Doney, S. C., Takahashi, T., Lee, K., Feely, R. A., Sabine, C.  
960 L., Triñanes, J. and Lima, I. D.: Variability of global net sea–air CO<sub>2</sub> fluxes over the last  
961 three decades using empirical relationships, *Tellus B*, 62(5), 352–368, doi:10.1111/j.1600-  
962 0889.2010.00498.x, 2010.
- 963 Patra, P. K., Canadell, J. G., Houghton, R. A., Piao, S. L., Oh, N.-H., Ciais, P., Manjunath, K.  
964 R., Chhabra, A., Wang, T., Bhattacharya, T., Bousquet, P., Hartman, J., Ito, A., Mayorga, E.,  
965 Niwa, Y., Raymond, P. A., Sarma, V. V. S. S. and Lasco, R.: The carbon budget of South  
966 Asia, *Biogeosciences*, 10(1), 513–527, doi:10.5194/bg-10-513-2013, 2013.
- 967 Patra, P. K., Houweling, S., Krol, M., Bousquet, P., Belikov, D., Bergmann, D., Bian, H.,  
968 Cameron-Smith, P., Chipperfield, M. P., Corbin, K., Fortems-Cheiney, A., Fraser, A., Gloor,  
969 E., Hess, P., Ito, A., Kawa, S. R., Law, R. M., Loh, Z., Maksyutov, S., Meng, L., Palmer, P. I.,

- 970 Prinn, R. G., Rigby, M., Saito, R. and Wilson, C.: TransCom model simulations of CH<sub>4</sub> and  
971 related species: linking transport, surface flux and chemical loss with CH<sub>4</sub> variability in the  
972 troposphere and lower stratosphere, *Atmos. Chem. Phys.*, 11(24), 12813–12837,  
973 doi:10.5194/acp-11-12813-2011, 2011.
- 974 Patra, P. K., Law, R. M., Peters, W., Rödenbeck, C., Takigawa, M., Aulagnier, C., Baker, I.,  
975 Bergmann, D. J., Bousquet, P., Brandt, J., Bruhwiler, L., Cameron-Smith, P. J., Christensen, J.  
976 H., Delage, F., Denning, A. S., Fan, S., Geels, C., Houweling, S., Imasu, R., Karstens, U.,  
977 Kawa, S. R., Kleist, J., Krol, M. C., Lin, S.-J., Lokupitiya, R., Maki, T., Maksyutov, S., Niwa,  
978 Y., Onishi, R., Parazoo, N., Pieterse, G., Rivier, L., Satoh, M., Serrar, S., Taguchi, S.,  
979 Vautard, R., Vermeulen, A. T. and Zhu, Z.: TransCom model simulations of hourly  
980 atmospheric CO<sub>2</sub>: Analysis of synoptic-scale variations for the period 2002–2003, *Global*  
981 *Biogeochem. Cycles*, 22(4), GB4013, doi:10.1029/2007GB003081, 2008.
- 982 Patra, P. K., Takigawa, M., Dutton, G. S., Uhse, K., Ishijima, K., Lintner, B. R., Miyazaki, K.  
983 and Elkins, J. W.: Transport mechanisms for synoptic, seasonal and interannual SF<sub>6</sub>  
984 variations and “age” of air in troposphere, *Atmos. Chem. Phys.*, 9(4), 1209–1225,  
985 doi:10.5194/acp-9-1209-2009, 2009a.
- 986 Patra, P., Takigawa, M., Ishijima, K., Choi, B.-C., Cunnold, D., J. Dlugokencky, E., Fraser,  
987 P., J. Gomez-Pelaez, A., Goo, T.-Y., Kim, J.-S., Krummel, P., Langenfelds, R., Meinhardt, F.,  
988 Mukai, H., O’Doherty, S., G. Prinn, R., Simmonds, P., Steele, P., Tohjima, Y., Tsuboi, K.,  
989 Uhse, K., Weiss, R., Worthy, D. and Nakazawa, T.: Growth rate, seasonal, synoptic, diurnal  
990 variations and budget of methane in the lower atmosphere, *J. Meteorol. Soc. Japan. Ser. II*,  
991 87(4), 635–663, 2009b.
- 992 Peng, S., Ciais, P., Chevallier, F., Peylin, P., Cadule, P., Sitch, S., Piao, S., Ahlström, A.,  
993 Huntingford, C., Levy, P., Li, X., Liu, Y., Lomas, M., Poulter, B., Viovy, N., Wang, T.,  
994 Wang, X., Zaehle, S., Zeng, N., Zhao, F. and Zhao, H.: Benchmarking the seasonal cycle of  
995 CO<sub>2</sub> fluxes simulated by terrestrial ecosystem models, *Global Biogeochem. Cycles*, 29(1),  
996 46–64, doi:10.1002/2014GB004931, 2015.
- 997 Peng, S. S., Piao, S. L., Bousquet, P., Ciais, P., Li, B. G., Lin, X., Tao, S., Wang, Z. P.,  
998 Zhang, Y. and Zhou, F.: Inventory of anthropogenic methane emissions in Mainland China  
999 from 1980 to 2010, *Atmos. Chem. Phys. Discuss.*, 2016, 1–29, doi:10.5194/acp-2016-139,  
1000 2016.
- 1001 Pérez-Landa, G., Ciais, P., Sanz, M. J., Gioli, B., Miglietta, F., Palau, J. L., Gangoiti, G. and  
1002 Millán, M. M.: Mesoscale circulations over complex terrain in the Valencia coastal region,  
1003 Spain – Part 1: Simulation of diurnal circulation regimes, *Atmos. Chem. Phys.*, 7(7), 1835–  
1004 1849, doi:10.5194/acp-7-1835-2007, 2007.
- 1005 Peters, W., Krol, M. C., Dlugokencky, E. J., Dentener, F. J., Bergamaschi, P., Dutton, G.,  
1006 Velthoven, P. v., Miller, J. B., Bruhwiler, L. and Tans, P. P.: Toward regional-scale modeling  
1007 using the two-way nested global model TM5: Characterization of transport using SF<sub>6</sub>, *J.*  
1008 *Geophys. Res. Atmos.*, 109(D19), D19314, doi:10.1029/2004JD005020, 2004.
- 1009 Peters, W., Krol, M. C., Van Der Werf, G. R., Houweling, S., Jones, C. D., Hughes, J.,  
1010 Schaefer, K., Masarie, K. A., Jacobson, A. R., Miller, J. B., Cho, C. H., Ramonet, M.,  
1011 Schmidt, M., Ciattaglia, L., Apadula, F., Heltai, D., Meinhardt, F., Di Sarra, A. G., Piacentino,  
1012 S., Sferlazzo, D., Aalto, T., Hatakka, J., Ström, J., Haszpra, L., Meijer, H. A. J., Van der  
1013 Laan, S., Neubert, R. E. M., Jordan, A., Rodó, X., Morguá, J.-A., Vermeulen, A. T., Popa, E.,  
1014 Rozanski, K., Zimnoch, M., Manning, A. C., Leuenberger, M., Uglietti, C., Dolman, A. J.,

- 1015 Ciais, P., Heimann, M. and Tans, P. P.: Seven years of recent European net terrestrial carbon  
1016 dioxide exchange constrained by atmospheric observations, *Glob. Chang. Biol.*, 16(4), 1317–  
1017 1337, doi:10.1111/j.1365-2486.2009.02078.x, 2010.
- 1018 Pillai, D., Gerbig, C., Ahmadov, R., Rödenbeck, C., Kretschmer, R., Koch, T., Thompson, R.,  
1019 Neininger, B. and Lavrié, J. V: High-resolution simulations of atmospheric CO<sub>2</sub> over  
1020 complex terrain – representing the Ochsenkopf mountain tall tower, *Atmos. Chem. Phys.*,  
1021 11(15), 7445–7464, doi:10.5194/acp-11-7445-2011, 2011.
- 1022 Popa, M. E., Gloor, M., Manning, A. C., Jordan, A., Schultz, U., Haensel, F., Seifert, T. and  
1023 Heimann, M.: Measurements of greenhouse gases and related tracers at Bialystok tall tower  
1024 station in Poland, *Atmos. Meas. Tech.*, 3(2), 407–427, doi:10.5194/amt-3-407-2010, 2010.
- 1025 Pregger, T., Scholz, Y. and Friedrich, R.: Documentation of the anthropogenic GHG  
1026 emission data for Europe provided in the Frame of CarboEurope GHG and CarboEurope IP,  
1027 Stuttgart, Germany., 2007.
- 1028 Le Quéré, C., Moriarty, R., Andrew, R. M., Canadell, J. G., Sitch, S., Korsbakken, J. I.,  
1029 Friedlingstein, P., Peters, G. P., Andres, R. J., Boden, T. A., Houghton, R. A., House, J. I.,  
1030 Keeling, R. F., Tans, P., Arneeth, A., Bakker, D. C. E., Barbero, L., Bopp, L., Chang, J.,  
1031 Chevallier, F., Chini, L. P., Ciais, P., Fader, M., Feely, R. A., Gkritzalis, T., Harris, I., Hauck,  
1032 J., Ilyina, T., Jain, A. K., Kato, E., Kitidis, V., Klein Goldewijk, K., Koven, C., Landschützer,  
1033 P., Lauvset, S. K., Lefèvre, N., Lenton, A., Lima, I. D., Metzl, N., Millero, F., Munro, D. R.,  
1034 Murata, A., Nabel, J. E. M. S., Nakaoka, S., Nojiri, Y., O’Brien, K., Olsen, A., Ono, T., Pérez,  
1035 F. F., Pfeil, B., Pierrot, D., Poulter, B., Rehder, G., Rödenbeck, C., Saito, S., Schuster, U.,  
1036 Schwinger, J., Séférian, R., Steinhoff, T., Stocker, B. D., Sutton, A. J., Takahashi, T.,  
1037 Tilbrook, B., van der Laan-Luijkx, I. T., van der Werf, G. R., van Heuven, S., Vandemark, D.,  
1038 Viovy, N., Wiltshire, A., Zaehle, S. and Zeng, N.: Global Carbon Budget 2015, *Earth Syst.*  
1039 *Sci. Data*, 7(2), 349–396, doi:10.5194/essd-7-349-2015, 2015.
- 1040 Ramonet, M., Ciais, P., Nepomniachii, I., Sidorov, K., Neubert, R. E. M., Langendörfer, U.,  
1041 Picard, D., Kazan, V., Biraud, S., Gusti, M., Kolle, O., Schulze, E.-D. and Lloyd, J.: Three  
1042 years of aircraft-based trace gas measurements over the Fyodorovskoye southern taiga forest,  
1043 300 km north-west of Moscow, *Tellus B*, 54(5), 713–734, doi:10.1034/j.1600-  
1044 0889.2002.01358.x, 2002.
- 1045 Randerson, J. T., Chen, Y., van der Werf, G. R., Rogers, B. M. and Morton, D. C.: Global  
1046 burned area and biomass burning emissions from small fires, *J. Geophys. Res.*  
1047 *Biogeosciences*, 117(G4), n/a-n/a, doi:10.1029/2012JG002128, 2012.
- 1048 Ridgwell, A. J., Marshall, S. J. and Gregson, K.: Consumption of atmospheric methane by  
1049 soils: A process-based model, *Global Biogeochem. Cycles*, 13(1), 59–70,  
1050 doi:10.1029/1998GB900004, 1999.
- 1051 Rio, C., Hourdin, F., Rio, C. and Hourdin, F.: A Thermal Plume Model for the Convective  
1052 Boundary Layer: Representation of Cumulus Clouds, *J. Atmos. Sci.*, 65(2), 407–425,  
1053 doi:10.1175/2007JAS2256.1, 2008.
- 1054 Rödenbeck, C., Houweling, S., Gloor, M. and Heimann, M.: CO<sub>2</sub> flux history 1982–2001  
1055 inferred from atmospheric data using a global inversion of atmospheric transport, *Atmos.*  
1056 *Chem. Phys.*, 3(6), 1919–1964, doi:10.5194/acp-3-1919-2003, 2003.
- 1057 Saeki, T., Saito, R., Belikov, D. and Maksyutov, S.: Global high-resolution simulations of  
1058 CO<sub>2</sub> and CH<sub>4</sub> using a NIES transport model to produce a priori concentrations for use in



- 1059 satellite data retrievals, *Geosci. Model Dev.*, 6(1), 81–100, doi:10.5194/gmd-6-81-2013, 2013.
- 1060 Sanderson, M. G.: Biomass of termites and their emissions of methane and carbon dioxide: A  
1061 global database, *Global Biogeochem. Cycles*, 10(4), 543–557, doi:10.1029/96GB01893, 1996.
- 1062 Sasakawa, M., Shimoyama, K., Machida, T., Tsuda, N., Suto, H., Arshinov, M., Davydov, D.,  
1063 Fofonov, A., Krasnov, O., Saeki, T., Koyama, Y. and Maksyutov, S.: Continuous  
1064 measurements of methane from a tower network over Siberia, *Tellus B*, 62(5), 403–416,  
1065 doi:10.1111/j.1600-0889.2010.00494.x, 2010.
- 1066 Swathi, P. S., Indira, N. K., Rayner, P. J., Ramonet, M., Jagadheesha, D., Bhatt, B. C. and  
1067 Gaur, V. K.: Robust inversion of carbon dioxide fluxes over temperate Eurasia in 2006–2008,  
1068 *Curr. Sci.*, 105(2), 201–208, 2013.
- 1069 Szopa, S., Balkanski, Y., Schulz, M., Bekki, S., Cugnet, D., Fortems-Cheiney, A., Turquety,  
1070 S., Cozic, A., Déandreis, C., Hauglustaine, D., Idelkadi, A., Lathière, J., Lefevre, F.,  
1071 Marchand, M., Vuolo, R., Yan, N. and Dufresne, J.-L.: Aerosol and ozone changes as forcing  
1072 for climate evolution between 1850 and 2100, *Clim. Dyn.*, 40(9–10), 2223–2250,  
1073 doi:10.1007/s00382-012-1408-y, 2013.
- 1074 Taylor, K. E.: Summarizing multiple aspects of model performance in a single diagram, *J.*  
1075 *Geophys. Res. Atmos.*, 106(D7), 7183–7192, doi:10.1029/2000JD900719, 2001.
- 1076 Thompson, R. L., Ishijima, K., Saikawa, E., Corazza, M., Karstens, U., Patra, P. K.,  
1077 Bergamaschi, P., Chevallier, F., Dlugokencky, E., Prinn, R. G., Weiss, R. F., O’Doherty, S.,  
1078 Fraser, P. J., Steele, L. P., Krummel, P. B., Vermeulen, A., Tohjima, Y., Jordan, A., Haszpra,  
1079 L., Steinbacher, M., Van der Laan, S., Aalto, T., Meinhardt, F., Popa, M. E., Moncrieff, J.  
1080 and Bousquet, P.: TransCom N<sub>2</sub>O model inter-comparison – Part 2: Atmospheric inversion  
1081 estimates of N<sub>2</sub>O emissions, *Atmos. Chem. Phys.*, 14(12), 6177–6194, doi:10.5194/acp-14-  
1082 6177-2014, 2014.
- 1083 Thompson, R. L., Patra, P. K., Chevallier, F., Maksyutov, S., Law, R. M., Ziehn, T., van der  
1084 Laan-Luijkx, I. T., Peters, W., Ganshin, A., Zhuravlev, R., Maki, T., Nakamura, T., Shirai, T.,  
1085 Ishizawa, M., Saeki, T., Machida, T., Poulter, B., Canadell, J. G. and Ciais, P.: Top-down  
1086 assessment of the Asian carbon budget since the mid 1990s, *Nat Commun*, 7 [online]  
1087 Available from: <http://dx.doi.org/10.1038/ncomms10724>, 2016.
- 1088 Thompson, R. L., Stohl, A., Zhou, L. X., Dlugokencky, E., Fukuyama, Y., Tohjima, Y., Kim,  
1089 S.-Y., Lee, H., Nisbet, E. G., Fisher, R. E., Lowry, D., Weiss, R. F., Prinn, R. G., O’Doherty,  
1090 S., Young, D. and White, J. W. C.: Methane emissions in East Asia for 2000–2011 estimated  
1091 using an atmospheric Bayesian inversion, *J. Geophys. Res. Atmos.*, 120(9), 4352–4369,  
1092 doi:10.1002/2014JD022394, 2015.
- 1093 Thoning, K. W., Tans, P. P. and Komhyr, W. D.: Atmospheric carbon dioxide at Mauna Loa  
1094 Observatory: 2. Analysis of the NOAA GMCC data, 1974–1985, *J. Geophys. Res. Atmos.*,  
1095 94(D6), 8549–8565, doi:10.1029/JD094iD06p08549, 1989.
- 1096 Tian, H., Lu, C., Ciais, P., Michalak, A. M., Canadell, J. G., Saikawa, E., Huntzinger, D. N.,  
1097 Gurney, K. R., Sitch, S., Zhang, B., Yang, J., Bousquet, P., Bruhwiler, L., Chen, G.,  
1098 Dlugokencky, E., Friedlingstein, P., Melillo, J., Pan, S., Poulter, B., Prinn, R., Saunio, M.,  
1099 Schwalm, C. R. and Wofsy, S. C.: The terrestrial biosphere as a net source of greenhouse  
1100 gases to the atmosphere, *Nature*, 531(7593), 225–228 [online] Available from:  
1101 <http://dx.doi.org/10.1038/nature16946>, 2016.

- 1102 Tiedtke, M.: A Comprehensive mass flux scheme for cumulus parameterization in large-scale  
1103 models, *Mon. Weather Rev.*, 117(8), 1779–1800, doi:10.1175/1520-  
1104 0493(1989)117<1779:ACMFSF>2.0.CO, 1989.
- 1105 Tiwari, Y. K. and Kumar, R. K.: GHG observation programs in India, *Asian GAW Greenh.*  
1106 *Gases Newsl.*, No.3, 5–11, 2012.
- 1107 Tiwari, Y. K., Vellore, R. K., Ravi Kumar, K., van der Schoot, M. and Cho, C.-H.: Influence  
1108 of monsoons on atmospheric CO<sub>2</sub> spatial variability and ground-based monitoring over India,  
1109 *Sci. Total Environ.*, 490(0), 570–578, doi:http://dx.doi.org/10.1016/j.scitotenv.2014.05.045,  
1110 2014.
- 1111 Wada, A., Matsueda, H., Sawa, Y., Tsuboi, K. and Okubo, S.: Seasonal variation of  
1112 enhancement ratios of trace gases observed over 10 years in the western North Pacific, *Atmos.*  
1113 *Environ.*, 45(12), 2129–2137, doi:http://dx.doi.org/10.1016/j.atmosenv.2011.01.043, 2011.
- 1114 Wang, J.-W., Denning, A. S., Lu, L., Baker, I. T., Corbin, K. D. and Davis, K. J.:  
1115 Observations and simulations of synoptic, regional, and local variations in atmospheric CO<sub>2</sub>,  
1116 *J. Geophys. Res. Atmos.*, 112(D4), D04108, doi:10.1029/2006JD007410, 2007.
- 1117 Wang, R., Balkanski, Y., Boucher, O., Ciais, P., Schuster, G. L., Chevallier, F., Samset, B. H.,  
1118 Liu, J., Piao, S., Valari, M. and Tao, S.: Estimation of global black carbon direct radiative  
1119 forcing and its uncertainty constrained by observations, *J. Geophys. Res. Atmos.*, 121(10),  
1120 5948–5971, doi:10.1002/2015JD024326, 2016.
- 1121 Wang, R., Tao, S., Balkanski, Y., Ciais, P., Boucher, O., Liu, J., Piao, S., Shen, H., Vuolo, M.  
1122 R., Valari, M., Chen, H., Chen, Y., Cozic, A., Huang, Y., Li, B., Li, W., Shen, G., Wang, B.  
1123 and Zhang, Y.: Exposure to ambient black carbon derived from a unique inventory and high-  
1124 resolution model, *Proc. Natl. Acad. Sci.* [online] Available from:  
1125 <http://www.pnas.org/content/early/2014/01/23/1318763111.abstract>, 2014.
- 1126 Wei, Y., Liu, S., Huntzinger, D. N., Michalak, A. M., Viovy, N., Post, W. M., Schwalm, C.  
1127 R., Schaefer, K., Jacobson, A. R., Lu, C., Tian, H., Ricciuto, D. M., Cook, R. B., Mao, J. and  
1128 Shi, X.: The North American Carbon Program Multi-scale Synthesis and Terrestrial Model  
1129 Intercomparison Project – Part 2: Environmental driver data, *Geosci. Model Dev.*, 7(6),  
1130 2875–2893, doi:10.5194/gmd-7-2875-2014, 2014.
- 1131 Van Der Werf, G. R., Randerson, J. T., Giglio, L., Van Leeuwen, T. T., Chen, Y., Rogers, B.  
1132 M., Mu, M., Van Marle, M. J. E., Morton, D. C., Collatz, G. J., Yokelson, R. J. and  
1133 Kasibhatla, P. S.: Global fire emissions estimates during 1997–2016, *Earth Syst. Sci. Data*,  
1134 95194, 697–720, doi:10.5194/essd-9-697-2017, 2017.
- 1135 Winderlich, J., Chen, H., Gerbig, C., Seifert, T., Kolle, O., Lavrič, J. V, Kaiser, C., Höfer, A.  
1136 and Heimann, M.: Continuous low-maintenance CO<sub>2</sub>/CH<sub>4</sub>/H<sub>2</sub>O measurements at the Zotino  
1137 Tall Tower Observatory (ZOTTO) in Central Siberia, *Atmos. Meas. Tech.*, 3(4), 1113–1128,  
1138 doi:10.5194/amt-3-1113-2010, 2010.
- 1139 Yver Kwok, C., Laurent, O., Guemri, A., Philippon, C., Wastine, B., Rella, C. W., Vuillemin,  
1140 C., Truong, F., Delmotte, M., Kazan, V., Darding, M., Lebègue, B., Kaiser, C., Xueref-Rémy,  
1141 I. and Ramonet, M.: Comprehensive laboratory and field testing of cavity ring-down  
1142 spectroscopy analyzers measuring H<sub>2</sub>O, CO<sub>2</sub>, CH<sub>4</sub> and CO, *Atmos. Meas. Tech.*, 8(9), 3867–  
1143 3892, doi:10.5194/amt-8-3867-2015, 2015.
- 1144



1146 **Tables**

1147 **Table 1** The prescribed CH<sub>4</sub> and CO<sub>2</sub> surface fluxes used as model input. For each trace gas,  
 1148 magnitudes of different types of fluxes are given for the year 2010. Total<sub>global</sub> and Total<sub>zoom</sub>  
 1149 indicate the total flux summarized over the globe and the zoomed region, respectively.

Type of CH <sub>4</sub> fluxes	Temporal resolution	Spatial resolution	Total <sub>global</sub> (TgCH <sub>4</sub> /yr)	Total <sub>zoom</sub> (TgCH <sub>4</sub> /yr)	Data source
Anthropogenic – rice	Monthly, interannual	0.1°	38	32	EDGARv4.2FT2010 + Matthews et al (1991)
Anthropogenic – others	Yearly, interannual	0.1°	320	131	EDGARv4.2FT2010
Wetland	Monthly, climatological	1°	175	29	Kaplan et al. (2006)
Biomass burning	Monthly, interannual	0.5°	19	3	GFED v4.1
Termite	Monthly, climatological	1°	19	3	Sanderson et al. (1996)
Soil	Monthly, climatological	1°	-38	-7	Ridgwell et al. (1999)
Ocean	Monthly, climatological	1°	17	3	Lambert & Schmidt (1993)
Total, TgCH <sub>4</sub> /yr			550	194	
Type of CO <sub>2</sub> fluxes	Temporal resolution	Spatial resolution	Total <sub>global</sub> (PgC/yr)	Total <sub>zoom</sub> (PgC/yr)	Data source
Anthropogenic	Monthly, interannual	1°	8.9	3.6	IER-EDGAR product
Anthropogenic	Daily, interannual	1°			
Anthropogenic	Hourly, interannual	1°			
Biomass burning	Monthly, interannual	0.5°	2.0	0.2	GFED v4.1
Land flux (NEE)	Monthly, interannual	0.5°	-2.7	0.1	OCHIDEE outputs from trunk version r1882
Land flux (NEE)	Daily, interannual	0.5°			
Land flux (NEE)	Hourly, interannual	0.5°			
Ocean flux	Monthly, interannual	4°×5°	-1.3	0.1	NOAA/PMEL & AOML product; Park et al. (2010)
Total, PgC/yr			6.9	3.9	

1150

1151 **Table 2** Stations used in this study. For the column ‘Zoom’, ‘Y’ indicates a station within the zoomed region.

	Code	Station	LON (°)	LAT (°)	ALT (masl)	Contributor	Type	Time periods used in this study	Zoom	CH <sub>4</sub>	CO <sub>2</sub>
<u>1</u>	<u>ALT</u>	<u>Alert, Canada</u>	<u>-62.52</u>	<u>82.45</u>	<u>210</u>	<u>NOAA/ESRL</u>	<u>coastal</u>	<u>Flask: 2006–2013</u>		<u>Y</u>	<u>Y</u>
<u>2</u>	<u>AMS</u>	<u>Amsterdam Island, France</u>	<u>77.54</u>	<u>-37.80</u>	<u>70</u>	<u>LSCE</u>	<u>marine</u>	<u>Flask: 2006–2013</u>		<u>Y</u>	<u>Y</u>
<u>3</u>	AMY	Anmyeon-do, Korea	126.32	36.53	133	KMA	coastal	<u>Continuous: 2006–2013</u>	Y	Y	
<u>4</u>	BKT	Bukit Kototabang, Indonesia	100.32	-0.20	869	BMKG, Empa, NOAA/ESRL	<u>mountain</u>	Flask: 2006–2013 CH <sub>4</sub> continuous: 2009–2013 CO <sub>2</sub> continuous: 2010–2013	Y	Y	Y
<u>5</u>	<u>BRW</u>	<u>Barrow, USA</u>	<u>-156.60</u>	<u>71.32</u>	<u>11</u>	<u>NOAA/ESRL</u>	<u>coastal</u>	<u>Continuous: 2006–2013</u>		<u>Y</u>	<u>Y</u>
<u>6</u>	<u>CGO</u>	<u>Cape Grim, Australia</u>	<u>144.68</u>	<u>-40.68</u>	<u>94</u>	<u>NOAA/ESRL</u>	<u>marine</u>	<u>Flask: 2006–2013</u>		<u>Y</u>	<u>Y</u>
<u>7</u>	COI	Cape Ochi-ishi, Japan	145.50	43.16	94	NIES	coastal	<u>Continuous: 2006–2013</u>		Y	
<u>8</u>	CRI	Cape Rama, India	73.83	15.08	66	CSIRO	coastal	<u>Flask: 2009–2013</u>	Y	Y	Y
<u>9</u>	DDR	Mt. Dodaira, Japan	139.18	36.00	840	Saitama	<u>mountain</u>	<u>Continuous: 2006–2013</u>			Y
<u>10</u>	DSI	Dongsha Island, Taiwan, China	116.73	20.70	8	National Central Univ., NOAA/ESRL	marine	<u>Flask: 2010–2013</u>	Y	Y	Y
<u>11</u>	GMI	Mariana Island, Guam	144.66	13.39	5	Univ. of Guam, NOAA/ESRL	marine	<u>Flask: 2006–2013</u>		Y	Y
<u>12</u>	GSN	Gosan, Korea	126.12	33.15	144	NIER	marine	<u>Continous: 2006–2011</u>	Y	Y	Y
<u>13</u>	HAT	Hateruma, Japan	123.81	24.06	47	NIES	marine	<u>Continous: 2006–2013</u>	Y	Y	
<u>14</u>	HLE	Hanle, India	78.96	32.78	4517	LSCE, CSIR4PI, IIA	mountain	Flask: 2006–2013 CH <sub>4</sub> continuous: 2012–2013 CO <sub>2</sub> continuous: 2006–2013	Y	Y	Y
<u>15</u>	<u>JFJ</u>	<u>Jungfrauoch, Switzerland</u>	<u>7.99</u>	<u>46.55</u>	<u>3580</u>	<u>Empa</u>	<u>mountain</u>	<u>CH<sub>4</sub> continuous: 2006–2013</u> <u>CO<sub>2</sub> continuous: 2010–2013</u>		<u>Y</u>	<u>Y</u>
<u>16</u>	JIN	Jinsha, China	114.20	29.63	750	CMA	continental	<u>Flask: 2006–2011</u>	Y		Y
<u>17</u>	KIS	Kisai - Saitama	139.55	36.08	13	Saitama	continental	<u>Continous: 2006–2013</u>			Y
<u>18</u>	KZD	Sary Taukum, Kazakhstan	75.57	44.45	412	KSIEMC, NOAA/ESRL	continental	<u>Flask: 2006–2009</u>	Y	Y	Y
<u>19</u>	KZM	Plateau Assy, Kazakhstan	77.87	43.25	2524	KSIEMC, NOAA/ESRL	mountain	<u>Flask: 2006–2009</u>	Y	Y	Y
<u>20</u>	LIN	Lin’an, China	119.72	30.30	139	CMA	continental	<u>Flask: 2006–2011</u>	Y		Y
<u>21</u>	LLN	Lulin, Taiwan, China	120.87	23.47	2867	LAIBS, NOAA/ESRL	mountain	<u>Flask: 2006–2013</u>	Y	Y	Y
<u>22</u>	LON	Longfengshan, China	127.60	44.73	331	CMA	continental	<u>Flask: 2006–2011</u>	Y		Y
<u>23</u>	<u>MHD</u>	<u>Mace Head, Ireland</u>	<u>-9.90</u>	<u>53.33</u>	<u>8</u>	<u>NOAA/ESRL</u>	<u>coastal</u>	<u>Flask: 2006–2013</u>		<u>Y</u>	<u>Y</u>
<u>24</u>	MKW	Mikawa-Ichinomiya, Japan	137.43	34.85	50	Aichi	continental	<u>Continous: 2006–2011</u>	Y		Y

<a href="#">25</a>	<a href="#">MLO</a>	<a href="#">Mauna Loa, USA</a>	<a href="#">-155.58</a>	<a href="#">19.54</a>	<a href="#">3397</a>	<a href="#">NOAA/ESRL</a>	<a href="#">mountain</a>	<a href="#">Continuous: 2006–2013</a>		<a href="#">Y</a>	<a href="#">Y</a>
<a href="#">26</a>	MNM	Minamitori-shima, Japan	153.98	24.28	28	JMA	marine	<a href="#">Continuous: 2006–2013</a>		Y	Y
<a href="#">27</a>	<a href="#">NWR</a>	<a href="#">Niwot Ridge, USA</a>	<a href="#">-105.59</a>	<a href="#">40.05</a>	<a href="#">3523</a>	<a href="#">NOAA/ESRL</a>	<a href="#">mountain</a>	<a href="#">Flask: 2006–2013</a>		<a href="#">Y</a>	<a href="#">Y</a>
<a href="#">28</a>	PBL	Port Blair, India	92.76	11.65	20	LSCE, CSIR4PI, ESSO/NIOT	marine	<a href="#">Flask: 2009–2013</a>	Y	Y	Y
<a href="#">29</a>	PON	Pondicherry, India	79.86	12.01	30	LSCE, CSIR4PI, Pondicherry Univ.	coastal	Flask: 2006–2013 CH <sub>4</sub> continuous: 2011–2013 CO <sub>2</sub> continuous: 2011–2013	Y	Y	Y
<a href="#">30</a>	RYO	Ryori, Japan	141.82	39.03	280	JMA	continental	<a href="#">Continuous: 2006–2013</a>		Y	Y
<a href="#">31</a>	SDZ	Shangdianzi, China	117.12	40.65	293	CMA, NOAA/ESRL	continental	<a href="#">Flask: 2009–2013</a>	Y	Y	Y
<a href="#">32</a>	SEY	Mahe Island, Seychelles	55.53	-4.68	7	SBS, NOAA/ESRL	marine	<a href="#">Flask: 2006–2013</a>		Y	Y
<a href="#">33</a>	SNG	Sinhagad, India	73.75	18.35	1600	IITM	mountain	CH <sub>4</sub> flask: 2010–2013 CO <sub>2</sub> flask: 2009–2013	Y	Y	Y
<a href="#">34</a>	<a href="#">SPO</a>	<a href="#">South Pole, USA</a>	<a href="#">-24.80</a>	<a href="#">-89.98</a>	<a href="#">2810</a>	<a href="#">NOAA/ESRL</a>	<a href="#">mountain</a>	<a href="#">Flask: 2006–2013</a>		<a href="#">Y</a>	<a href="#">Y</a>
<a href="#">35</a>	TAP	Tae-ahn Peninsula, Korea	126.13	36.73	21	KCAER, NOAA/ESRL	coastal	<a href="#">Flask: 2006–2013</a>	Y	Y	Y
<a href="#">36</a>	UUM	Ulaan Uul, Mongolia	111.10	44.45	1012	MHRI, NOAA/ESRL	continental	<a href="#">Flask: 2006–2013</a>	Y	Y	Y
<a href="#">37</a>	WIS	Negev Desert, Israel	30.86	34.79	482	WIS, AIES, NOAA/ESRL	continental	<a href="#">Flask: 2006–2013</a>		Y	Y
<a href="#">38</a>	WLG	Mt. Waliguan, China	100.90	36.28	3890	CMA, NOAA/ESRL	mountain	<a href="#">Flask: 2006–2013</a>	Y	Y	Y
<a href="#">39</a>	YON	Yonagunijima, Japan	123.02	24.47	50	JMA	marine	<a href="#">Continuous: 2006–2013</a>	Y	Y	Y

1152

1153 Abbreviations:

1154 Aichi – Aichi Air Environment Division, Japan

1155 AIES – Arava Institute for Environmental Studies, Israel

1156 BMKG – Agency for Meteorology, Climatology and Geophysics, Indonesia

1157 CMA – China Meteorological Administration, China

1158 CSIR4PI – Council of Scientific and Industrial Research Fourth Paradigm Institute, India

1159 CSIRO – Commonwealth Scientific and Industrial Research Organisation, Australia

1160 Empa – Swiss Federal Laboratories for Materials Testing and Research, Switzerland

1161 ESSO/NIOT – Earth System Sciences Organisation/National Institute of Ocean Technology, India

1162 IIA – Indian Institute of Astrophysics, India

1163 IITM – Indian Institute of Tropical Meteorology, India

1164 JMA – Japan Meteorological Agency, Japan

1165 KCAER – Korea Centre for Atmospheric Environment Research, Republic of Korea

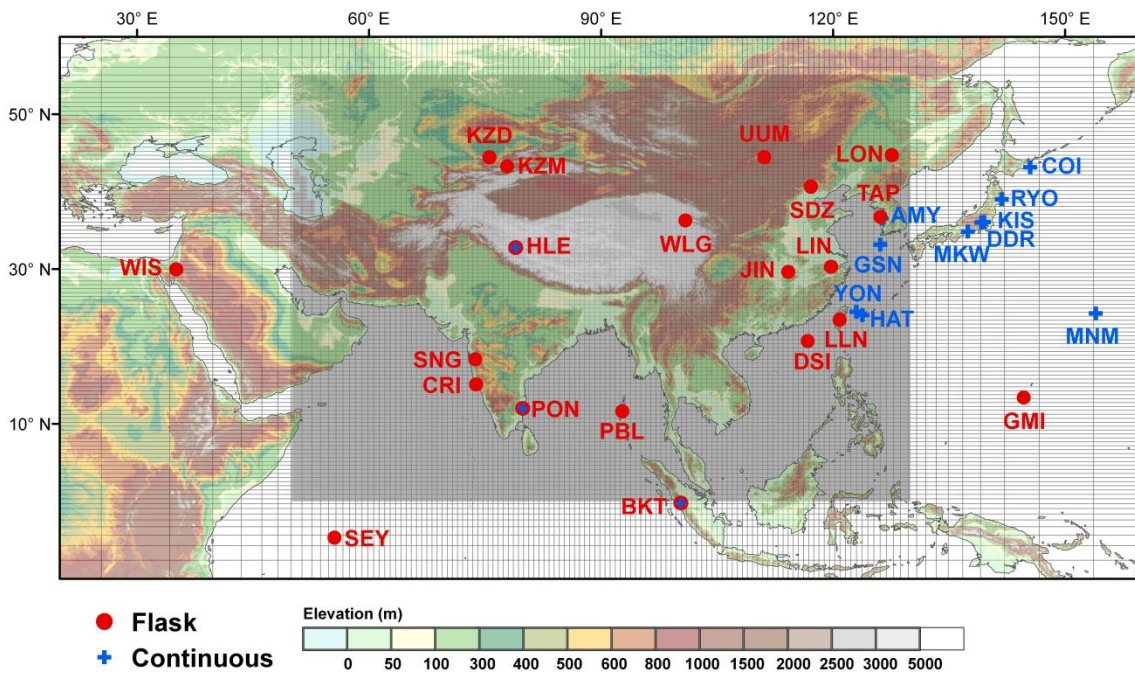
1166 KMA – Korea Meteorological Administration, Republic of Korea

1167 KSIEMC – Kazakh Scientific Institute of Environmental Monitoring and Climate, Kazakhstan

- 1168 LAIBS – Lulin Atmospheric Background Station, Taiwan
- 1169 LSCE – Laboratoire des Sciences du Climat et de l'Environnement, France
- 1170 MHRI – Mongolian Hydrometeorological Research Institute, Mongolia
- 1171 NIER – National Institute of Environmental Research, South Korea
- 1172 NIES – National Institute for Environmental Studies, Japan
- 1173 NIWA – National Institute of Water and Atmospheric Research, New Zealand
- 1174 NOAA/ESRL – National Oceanic and Atmospheric Administration/Earth System Research Laboratory
- 1175 Saitama – Center for Environmental Science in Saitama
- 1176 SBS – Seychelles Bureau of Standards, Seychelles
- 1177 WIS – Weizmann Institute of Science, Israel

1178 **Figures**

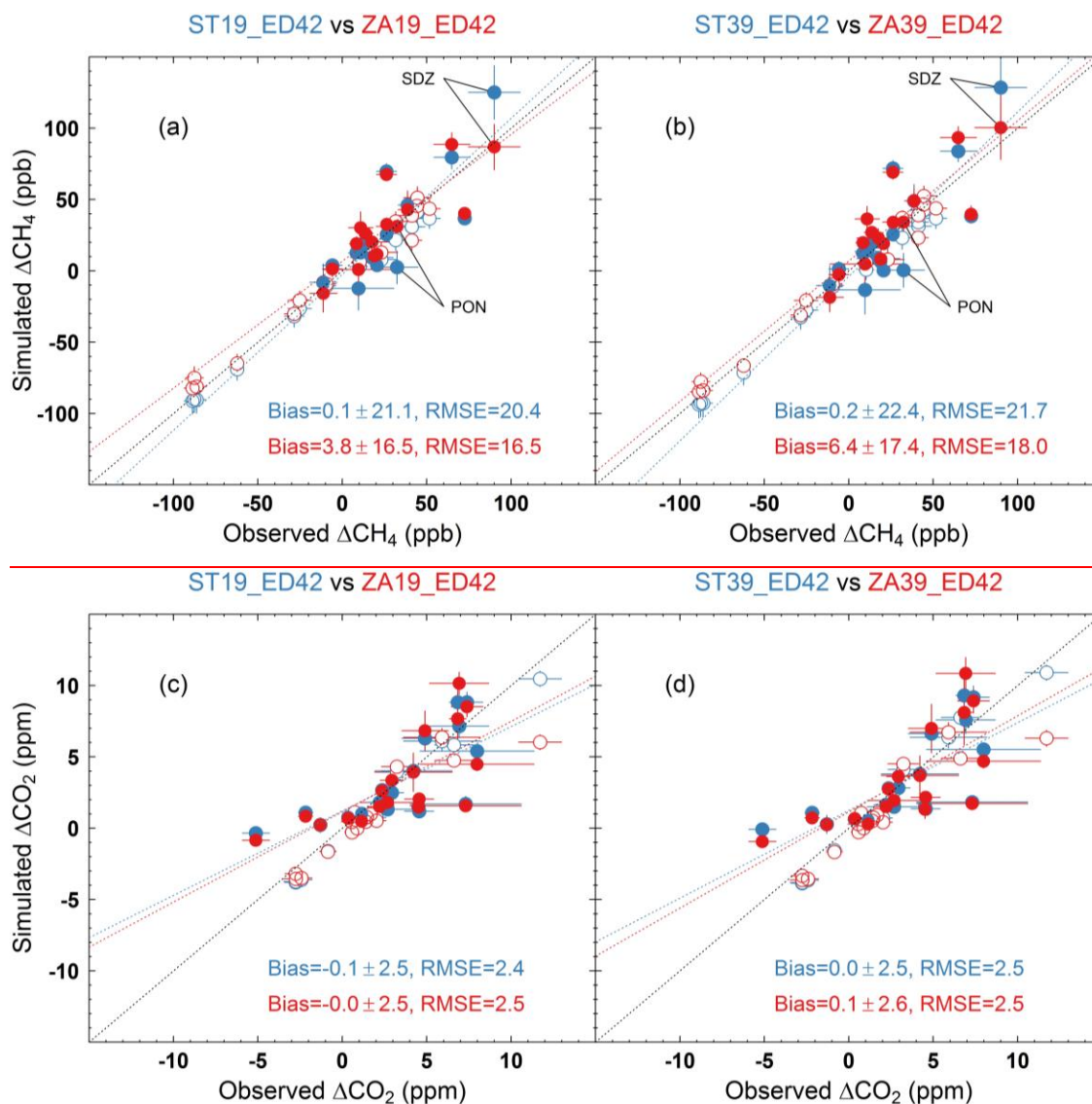
1179 | **Figure 1** Map of locations of stations within and around the zoomed region. The zoomed grid  
1180 | of the LMDz-INCA model is plotted with the NASA Shuttle Radar Topographic Mission  
1181 | (SRTM) 1km digital elevation data (DEM) as background (<http://srtm.csi.cgiar.org>). The grey  
1182 | shaded area indicates the region with a horizontal resolution of  $\sim 0.66^\circ \times \sim 0.51^\circ$ . The red  
1183 | close circle (blue cross) represents the atmospheric station where flask (continuous)  
1184 | measurements are available and used in this study.



1185  
1186



1187 **Figure 2** Scatterplots of the simulated and observed mean annual gradients of CH<sub>4</sub> (a, b) and  
 1188 CO<sub>2</sub> (c, d) between HLE and other stations. In each panel, the simulated CH<sub>4</sub> or CO<sub>2</sub>  
 1189 gradients are based on model outputs from STs (blue circles) and ZAs (red circles),  
 1190 respectively. The black dotted line indicates the identity line, whereas the blue and red dotted  
 1191 lines indicates the corresponding linear fitted lines. The closed and open circles represent  
 1192 stations inside and outside the zoomed region.



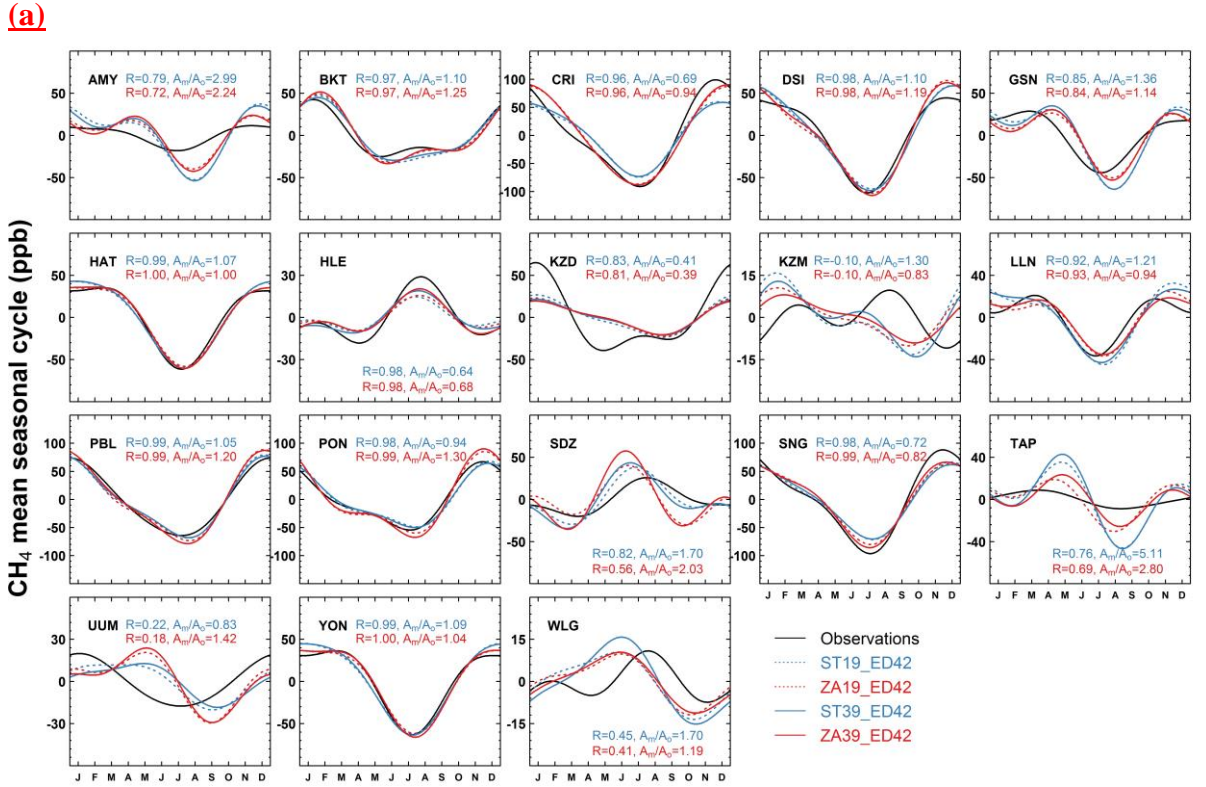
1193

1194

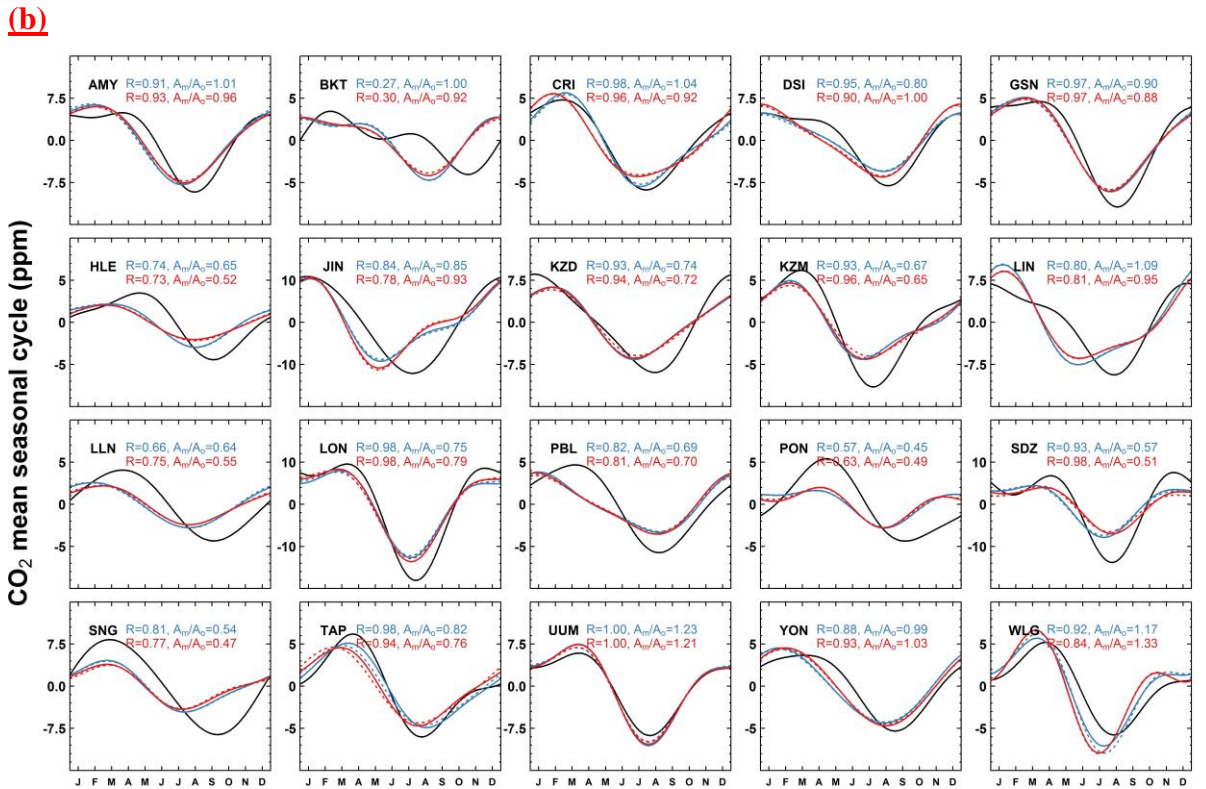
1195

1196  
1197  
1198  
1199  
1200

**Figure 3** The observed and simulated mean seasonal cycles of CH<sub>4</sub> (a) and CO<sub>2</sub> (b) for stations within the zoomed region. In each panel, the simulated mean seasonal cycles are based on model outputs from STs (blue lines) and ZAs (red lines), respectively. The text shows statistics between the simulated and observed seasonal cycles for 39-layer models.

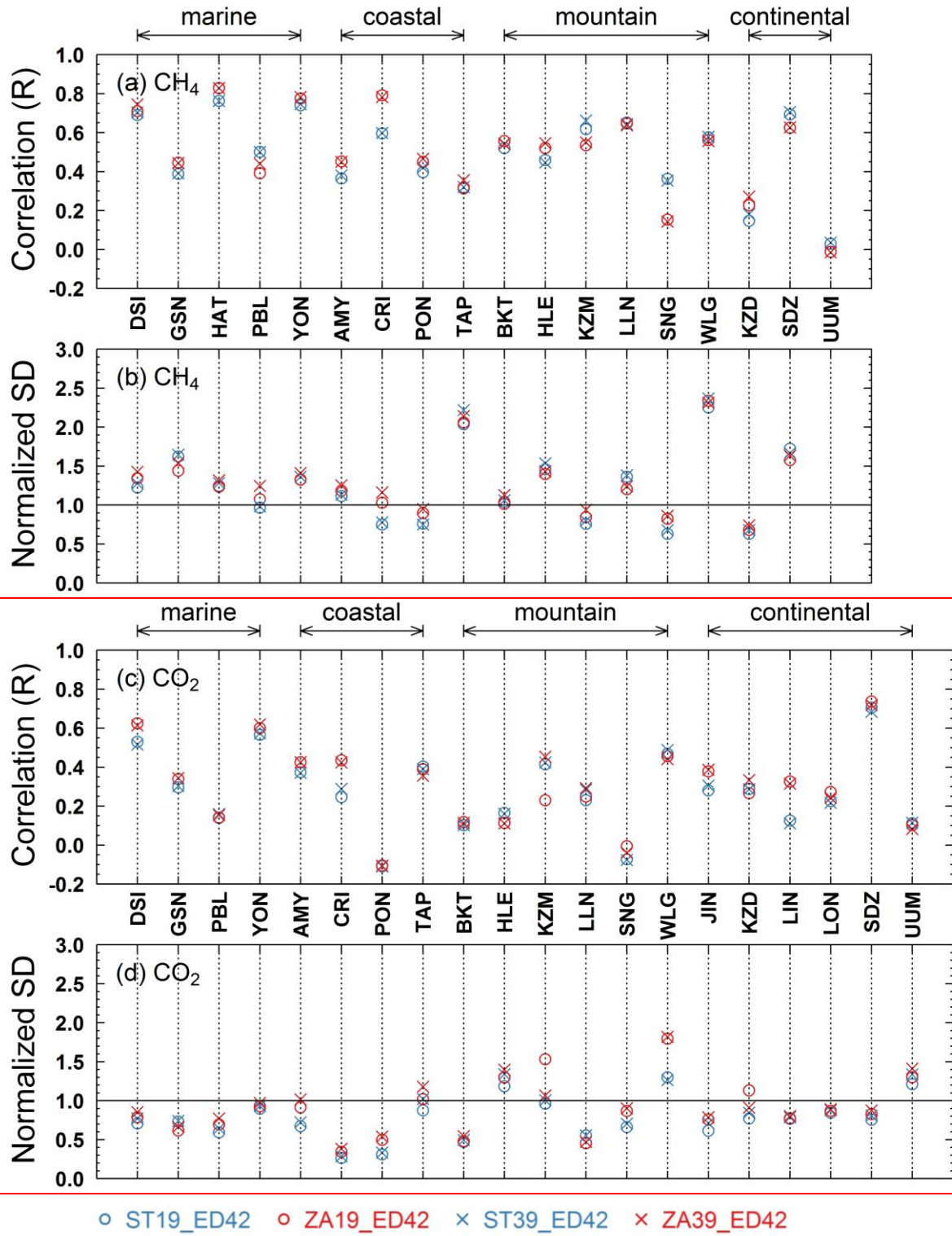


1201  
1202



1203

1204 **Figure 4** The correlations and normalized standard deviations between the simulated and  
 1205 observed synoptic variability for CH<sub>4</sub> (a,b) and CO<sub>2</sub> (c,d) at stations within the zoomed  
 1206 region. For each station, the synoptic variability is calculated from residuals from the  
 1207 smoothed fitting curve.



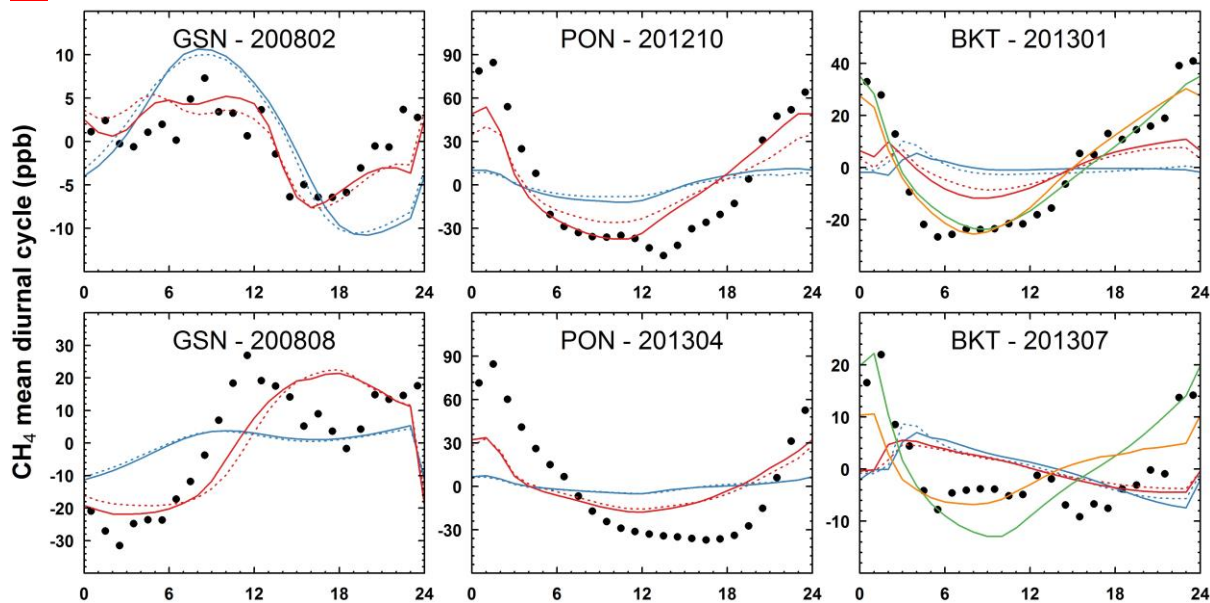
1208

1209

1210

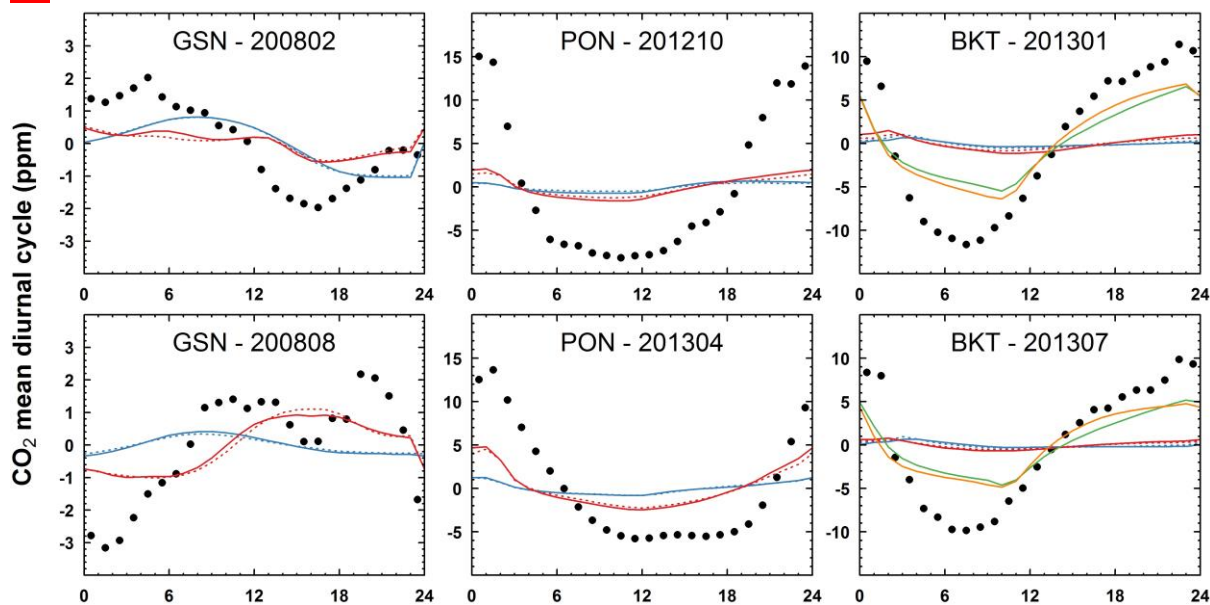
1211 **Figure 5** The observed and simulated mean diurnal cycles (in UTC time) of CH<sub>4</sub> (a) and CO<sub>2</sub>  
 1212 (b) at three stations within the zoomed region. For BKT, the simulated diurnal cycles at lower  
 1213 model levels are also presented.

1214 (a)



1215

1216 (b)



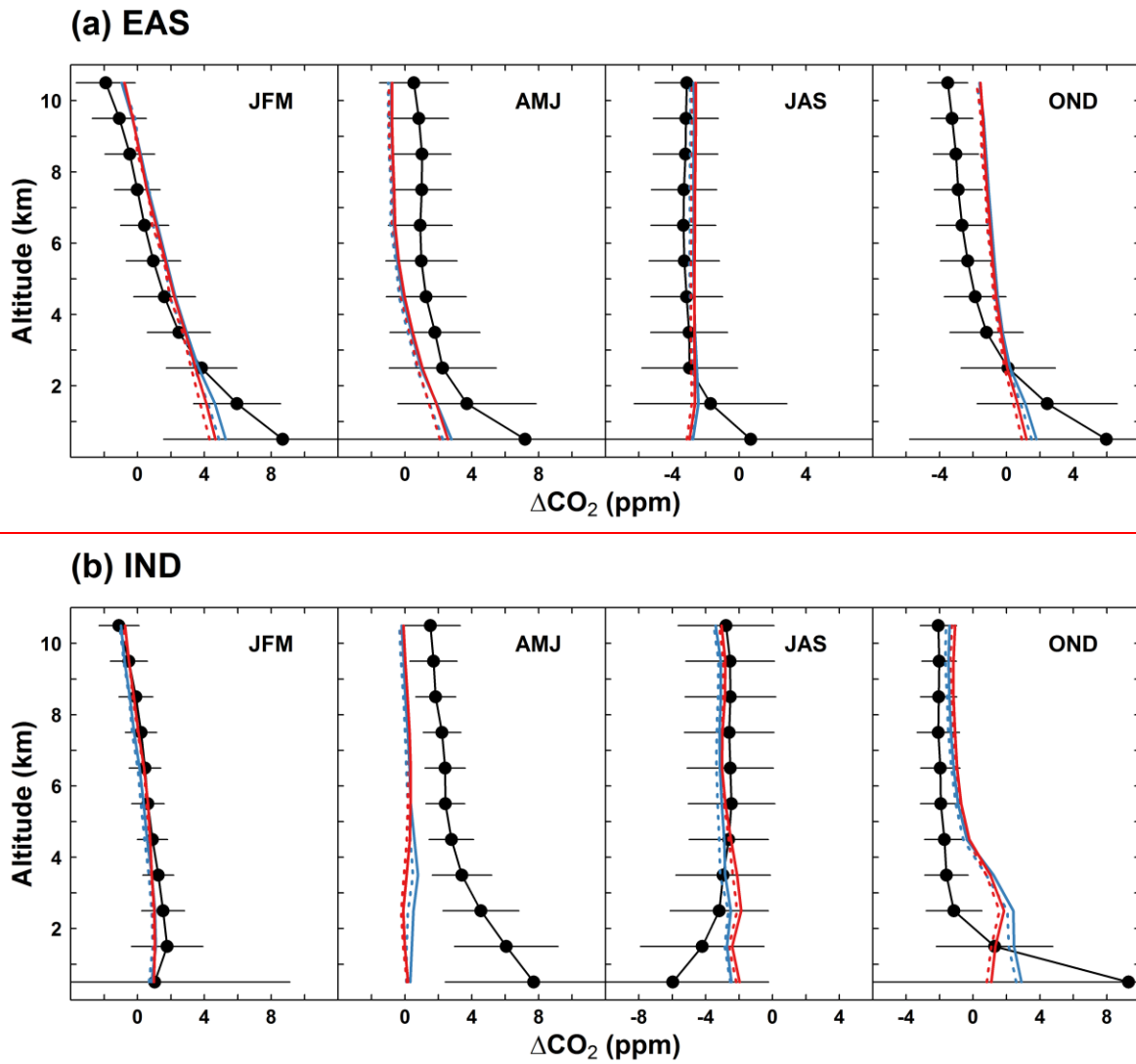
1217

- Observations
- ⋯ ST19\_ED42
- ⋯ ZA19\_ED42
- ST39\_ED42
- ZA39\_ED42
- ST39\_ED42, at lower model level
- ZA39\_ED42, at lower model level

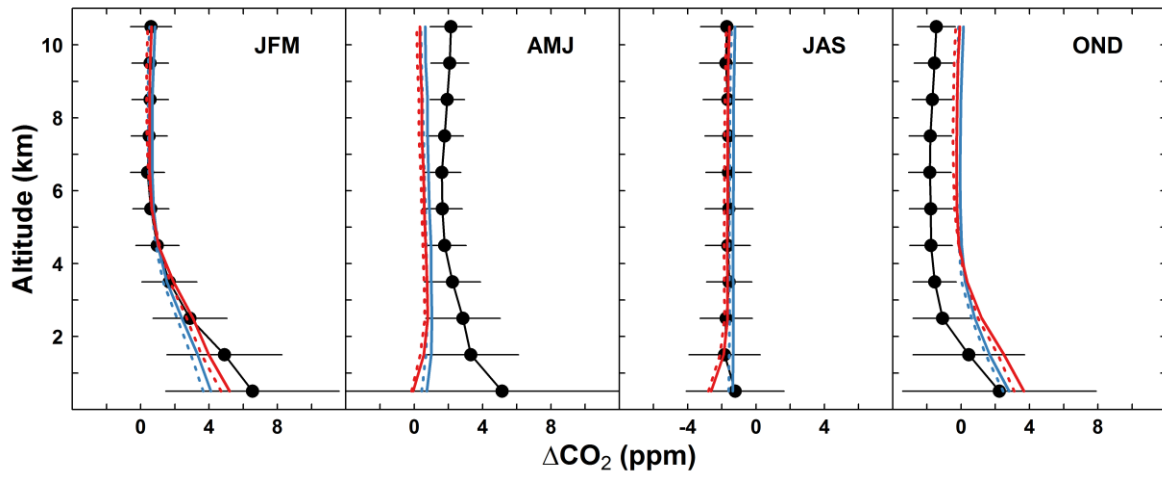
1218

1219

1220 **Figure 6** Seasonal mean observed and simulated CO<sub>2</sub> vertical profiles over (a) East Asia  
 1221 (EAS), (b) the Indian sub-continent (IND), (c) Northern Southeast Asia (NSA) and (d)  
 1222 Southern Southeast Asia (SSA). The observed vertical profiles are based on CO<sub>2</sub> continuous  
 1223 measurements onboard the commercial air flights from the CONTRAIL project during the  
 1224 period 2006–2011. For each 1-km altitude bin and each subregion, the observed and  
 1225 simulated time series are detrended (denoted as  $\Delta\text{CO}_2$ ) and seasonally averaged during  
 1226 January–March (JFM), April–June (AMJ), July–September (JAS) and October–December  
 1227 (OND).

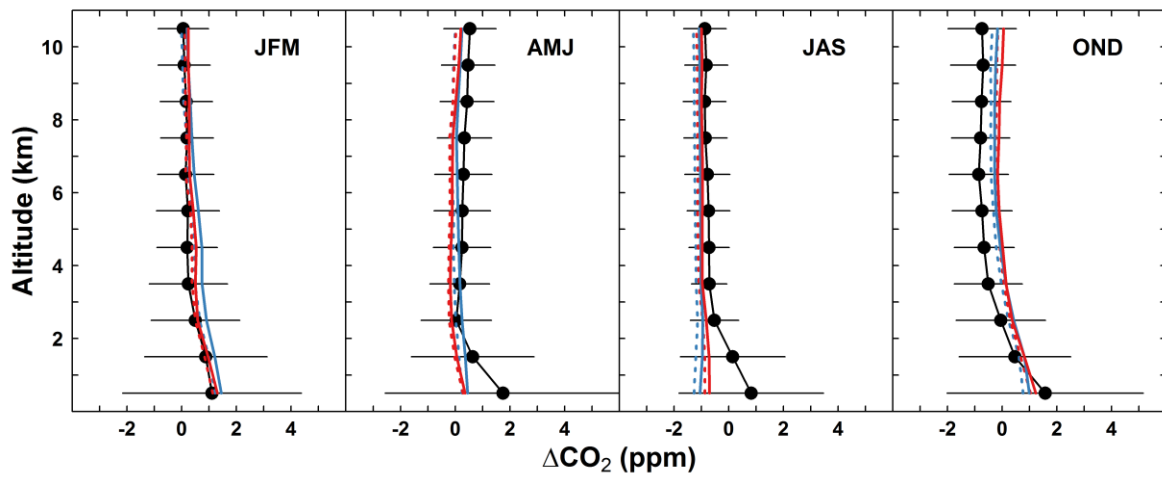


(c) NSA



1230

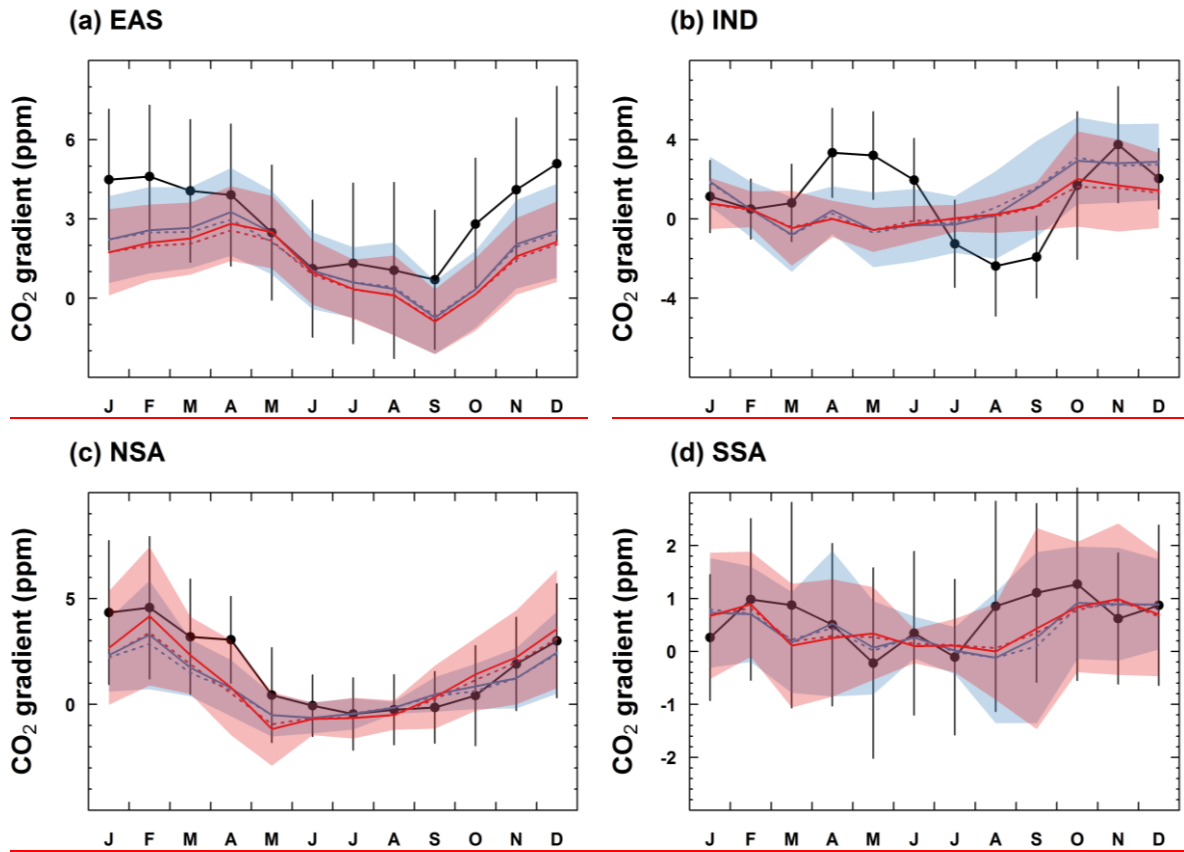
(d) SSA



1231

1232

1233 | **Figure 7** Monthly mean observed and simulated CO<sub>2</sub> gradient between 1 and 4km over (a)  
 1234 East Asia (EAS), (b) the Indian sub-continent (IND), (c) Northern Southeast Asia (NSA) and  
 1235 (d) Southern Southeast Asia (SSA). For each subregion, the monthly CO<sub>2</sub> gradients are  
 1236 calculated by averaging over all the vertical profiles the differences in CO<sub>2</sub> concentrations  
 1237 between 1 and 4km.



1238

1239

1240